

# Transformed Low-rank Adaptation via Tensor Decomposition and Its Applications to Text-to-image Models

Zerui Tao<sup>1,†</sup> Yuhta Takida<sup>2</sup> Naoki Murata<sup>2</sup> Qibin Zhao<sup>1</sup> Yuki Mitsufuji<sup>2,3</sup>

<sup>1</sup>RIKEN AIP <sup>2</sup>Sony AI <sup>3</sup>Sony Group Corporation

{zerui.tao, qibin.zhao}@riken.jp, {yuta.takida, naoki.murata, yuhki.mitsufuji}@sony.com

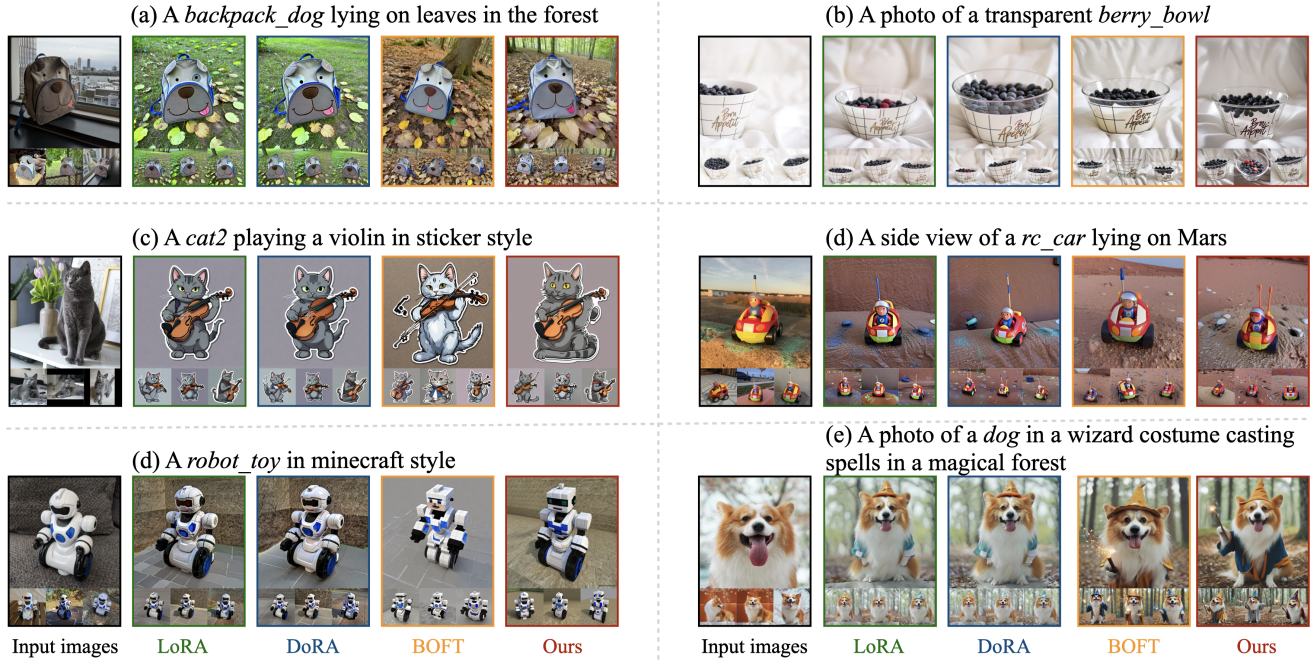


Figure 1. Qualitative comparison of the subject-driven generation results. Results are generated using fine-tuned checkpoint by each method. For each model, we randomly generate four images, all of which are shown here. The subcaptions are the given prompts, and the subjects in *italics* represent training subjects.

## Abstract

*Parameter-Efficient Fine-Tuning (PEFT) of text-to-image models has become an increasingly popular technique with many applications. Among the various PEFT methods, Low-Rank Adaptation (LoRA) and its variants have gained significant attention due to their effectiveness, enabling users to fine-tune models with limited computational resources. However, the approximation gap between the low-rank assumption and desired fine-tuning weights prevents the simultaneous acquisition of ultra-parameter-efficiency and better performance. To reduce this gap and further improve the power of LoRA, we propose a new PEFT method that combines two classes of adaptations, namely, transform and residual adaptations. In specific, we first apply*

*a full-rank and dense transform to the pre-trained weight. This learnable transform is expected to align the pre-trained weight as closely as possible to the desired weight, thereby reducing the rank of the residual weight. Then, the residual part can be effectively approximated by more compact and parameter-efficient structures, with a smaller approximation error. To achieve ultra-parameter-efficiency in practice, we design highly flexible and effective tensor decompositions for both the transform and residual adaptations. Additionally, popular PEFT methods such as DoRA can be summarized under this transform plus residual adaptation scheme. Experiments are conducted on fine-tuning Stable Diffusion models in subject-driven and controllable generation. The results manifest that our method can achieve better performances and parameter efficiency compared to LoRA and several baselines.*

<sup>†</sup>Work done during an internship at Sony AI

## 1. Introduction

In recent years, text-to-image generative models [8, 40, 43, 44, 47] have achieved remarkable results in image synthesis. In order to obtain the desired generative power, these models typically consist of hundreds of millions or even billions of parameters, which are trained on huge image and text datasets. Despite their incredible abilities, the high computational and memory costs largely prevent users from taking advantage of these models on their personalized or private datasets and tasks, such as subject-driven generation [10, 46], controllable generation [33, 62], and others [15, 56]. For subject-driven generation, users aim to adapt the pre-trained model to several images of the target subject, so that the model can generate new images of this subject given text prompts. Similarly, controllable generation involves fine-tuning the model on image, text, and control signal pairs, such as landmarks, segmentations and canny edges, to facilitate the ability of generation conditioned on these signals.

To circumvent the huge resource requirements for fine-tuning the text-to-image models, Parameter-Efficient Fine-Tuning (PEFT) has become an important research topic. In particular, Low-Rank Adaptation [LoRA, 18] and its variants have become the most widely adopted due to their simplicity, stability, and efficiency [9]. By assuming the fine-tuning adaptations have a low intrinsic rank, LoRA methods can greatly reduce the computational and memory costs by only updating the low-rank adaptation. While this simple approximation works surprisingly well, it still faces several challenges and issues. First, the low-rank approximation may yield a high recovery gap compared to the full fine-tuning adaptations, especially for difficult tasks [34]. Second, the simple matrix decomposition structure lacks flexibility in terms of adjusting the fine-tuning budget and further compression of large matrices. Therefore, both the fine-tuning performance and the parameter efficiency of LoRA tend to be sub-optimal and can be further improved.

To address these issues, we investigate a novel PEFT method called Transformed Low-Rank Adaptation (TLoRA) via tensor decomposition. The proposed method consists of two adaptation parts, namely, **Transform** and **Residual adaptations**. The **Transform adaptation** applies a linear transform to the pre-trained weight so that it can be projected into a space with a lower-rank fine-tuning process. This is necessary because the pre-trained weight may not have a low-rank fine-tuning weight. Subsequently, the **Residual adaptation** approximates the residual part using more compact and efficient structures. To effectively parameterize these adaptations, tensor decomposition techniques are adopted (as described below). Moreover, we empirically demonstrate the effectiveness of combining these two adaptations by investigating some pre-trained and fine-tuned models in Fig. 2 and Sec. 3.2.

**Transform adaptation.** The purpose of this learnable transform is to align the pre-trained weight as closely as possible to some target weight in order to reduce the rank of the residual adaptation. Since the target weight space (e.g., optimal weights for the fine-tuning task) is not likely to be low-rank, we assume the transform also has a full-rank structure. Furthermore, the transform is parameterized to be a dense matrix, allowing the information transmission among all neurons [28]. However, since this transform matrix is large, it should be represented by parameter-efficient structures. To meet all these requirements, we adopt the tensor-ring matrix [TRM, 7, 37, 66] format for the transform, which is a highly compact form for full-rank and dense matrices, as described in Sec. 3.3.

**Residual adaptation.** Assuming the effectiveness of the transform, the residual adaptation can be effectively approximated by more compact and parameter-efficient structures. While many efficient parameterizations are available, we focus on the tensor-ring decomposition [TR, 66] in this work. In our study, we implement TR using a different initialization strategy with previous PEFT literature using similar structures [2, 6, 59], showing that TR with the transform adaptation achieves promising performances with ultra-parameter-efficiency. Details are presented in Sec. 3.4

Additionally, in Sec. 3.5, we show that while some popular PEFT methods (e.g., DoRA [27] and Fourier-inspired LoRA [4, 11, 48]) adopt the idea of transform implicitly or explicitly, they are parameterized by either extremely sparse or fixed transforms, which may be insufficient.

To demonstrate the advantages of our model, we conduct experiments on two tasks, subject-driven generation and controllable generation, using Stable Diffusion XL [SDXL, 40] and Stable Diffusion [44] v1.5 models respectively. Compared to LoRA and several baselines, the results show that the transform part can effectively boost performances in most cases. Additionally, by using the compact tensor decompositions, our model is able to achieve desirable performances and ultra-parameter-efficiency simultaneously, e.g., fine-tuning SDXL with only 0.4M parameters in Fig. 1.

## 2. Related work

**Text-to-image model personalization.** Text-to-image generative models have shown exceptional results in image synthesis [8, 40, 43, 44, 47]. To personalize pre-trained models, Gal et al. [10] propose learning given subjects via textual inversion, while Ruiz et al. [46] fine-tune the whole model. ControlNet [62] incorporates an additional network branch that can learn datasets of paired control signals and images. While these methods [46, 62] may have large numbers of trainable parameters, Kumari et al. [22] show that fine-tuning the cross-attention layers alone is effective enough for these tasks. More recently, many works

have focused on developing PEFT methods for these tasks [4, 15, 16, 41, 55, 60, 65]. There are also training-free approaches [45], which could be slow at inference.

**Parameter-efficient fine-tuning.** Popular PEFT methods include Adapter [17], Prefix-tuning [26], Prompt-tuning [24], LoRA [18], and many of their variants. LoRA has become the most popular PEFT method due to its simplicity and impressive performances [9]. Many variants of LoRA have been proposed [19, 21, 27, 28, 34, 41, 63]. In DoRA [27], the pre-trained weight is decomposed into magnitude and direction, whereas vanilla LoRA is applied to the direction. In the current work, we show that DoRA can also be connected to our method as utilizing a diagonal transform. Orthogonal Fine-Tuning [OFT, 41] applies a learnable orthogonal transform for adaptation. However, for parameter efficiency, OFT adopts block diagonal matrices, which are highly sparse. Subsequently, many methods aim to improve OFT by applying particular dense transform structures [3, 28, 29, 61, 65]. Our method adopts a similar idea of using a transform, but we design a different dense matrix parameterization using tensor decomposition. Additionally, several works [4, 11, 48] also share similarities with ours by using *pre-defined and fixed* transforms.

**Tensor decomposition.** TD is a classical tool in signal processing and machine learning [7]. In particular, tensor-train [TT, 37] and its extension, tensor-ring [TR, 66], have shown exceptional results in model compression, including MLP [35], CNN [12, 52], RNN/LSTM [32, 38, 49, 58] and Transformer [30, 39]. Recently, TDs have also been applied to PEFT [2, 6, 20, 59]. While these works utilize similar TT/TR structures to our model, they do not apply the transform adaptation. Moreover, we study a different initialization strategy for the TR factors to make the training more stable, as we will show in our experiments.

### 3. Proposed model

#### 3.1. Preliminaries

**Notations.** Notations for tensors, matrices, vectors and scalars basically follow the conventions in the *Deep Learning* textbook [13, 14]. Furthermore, we use square brackets to denote entries or slices of an array. For example, given a tensor  $\mathbf{X} \in \mathbb{R}^{I \times J \times K}$ , we have matrix slices  $\mathbf{X}_{i::} = \mathbf{X}[i, :, :] \in \mathbb{R}^{J \times K}$ , vector slices  $\mathbf{x}_{i:j} = \mathbf{X}[i, j, :] \in \mathbb{R}^K$  and scalar entries  $x_{ijk} = \mathbf{X}[i, j, k] \in \mathbb{R}$ . We use  $\mathbf{I}_I$  to denote identity matrix of shape  $I \times I$ . The Kronecker product is denoted by  $\otimes$ . The matrix trace is denoted by  $\text{tr}(\cdot)$ .  $\text{diag}(\mathbf{m})$  denotes diagonal matrix with diagonal elements  $\mathbf{m}$ . For indices of tensorization, we adopt the little-endian convention [7]. For a vector  $\mathbf{x} \in \mathbb{R}^I$  with  $I = \prod_{d=1}^D I_d$ , if it is tensorized into  $\mathbf{X} \in \mathbb{R}^{I_1 \times \dots \times I_D}$ , we have  $\mathbf{x}[i_1 \dots i_D] = \mathbf{X}[i_1, \dots, i_D]$ , where  $i_1 \dots i_D = i_1 + (i_2 - 1)I_1 + (i_3 - 1)I_1 I_2 + \dots + (i_D - 1)I_1 \dots I_{D-1}$ .

**Low-rank adaptation [18].** Consider a linear layer  $\mathbf{y} = \mathbf{W}_0 \mathbf{x}$ , where the weight has shape  $I \times I$ . Given a pre-trained weight  $\mathbf{W}_0$ , LoRA aims to learn an additive adaptation  $\Delta$  of the same shape, i.e.,

$$\mathbf{y}' = (\mathbf{W}_0 + \Delta) \mathbf{x}, \quad s.t. \Delta = \mathbf{B} \mathbf{A}, \quad (1)$$

where the adaptation is parameterized by a low-rank matrix decomposition to reduce trainable parameters. The low-rank matrices  $\mathbf{B} \in \mathbb{R}^{I \times R}$  and  $\mathbf{A} \in \mathbb{R}^{R \times I}$  are optimized through the given fine-tuning tasks, and have a total of  $2IR$  trainable parameters, which is much smaller than the original size  $I^2$  if  $R \ll I$ . However, as some works [4, 34] indicate, the desired fine-tuning weight may not be low-rank.

**Orthogonal fine-tuning [41].** Instead of the additive adaptation in Eq. (1), OFT introduces an orthogonal transformation of the pre-trained weight for adaptation,

$$\mathbf{y}' = (\mathbf{W}_0 \mathbf{T}) \mathbf{x}, \quad (2)$$

where  $\mathbf{T}$  is a trainable orthogonal matrix of shape  $I \times I$ . However, directly optimizing  $\mathbf{T}$  is computationally infeasible due to its large size. In [41],  $\mathbf{T}$  is parameterized as a block diagonal matrix, which is extremely sparse for small parameter budgets. This sparsity is considered to reduce the information transfer and connectivity among neurons, which is deleterious to the fine-tuning. Therefore, parameter-efficient matrices with dense entries are more desirable for OFT [3, 28, 29, 61, 65].

#### 3.2. Our motivation

Supposing the target of fine-tuning is to approximate some desired weight  $\mathbf{W}_*$ , the assumption behind LoRA is that the difference  $\Delta_* = \mathbf{W}_* - \mathbf{W}_0$  is low-rank. However, this is unlikely to be true in real large foundation models [34].

Considering this approximation problem, if the target  $\Delta_*$  has a high rank, LoRA inevitably causes high approximation error, as illustrated in Figs. 2b and 2c. To address this issue, we first apply a learnable linear transform  $\mathbf{T}$  on  $\mathbf{W}_0$  to align  $\mathbf{W}_0$  on  $\mathbf{W}_*$  and then approximate the residual part by another compact structure. Here, the difference becomes  $\Delta'_* = \mathbf{W}_* - \mathbf{W}_0 \mathbf{T}$ . After the transform,  $\Delta'_*$  should have a smaller rank than the original  $\Delta_*$  so that we can use much more compact structures for approximation of this residual part. The overall fine-tuning structure becomes,

$$\mathbf{y}' = (\mathbf{W}_0 \mathbf{T} + \Delta) \mathbf{x}, \quad (3)$$

where  $\mathbf{T}$  and  $\Delta$  learnable compact parameterizations. To meet different requirements and desired properties, we design TRM form [37, 66] for the transform  $\mathbf{T}$  and TR form [37, 66] for the residual  $\Delta$  in Secs. 3.3 and 3.4 respectively.

To empirically illustrate the effectiveness of the transform, we conduct a simulation study on the pretrained

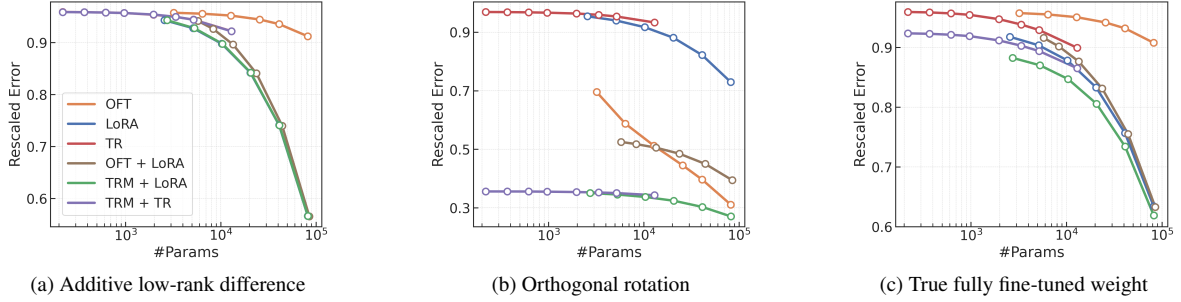


Figure 2. Simulation study on pre-trained SDXL [40] and fine-tuned SDXL-Inpaint [50] weights. SDXL-Inpaint is fine-tuned on image-mask pairs to facilitate imputation ability of the SDXL base model. We investigate the approximation of UNet attention layers, which are counterpart of our fine-tuning targets in experiments. We test the approximation error on three cases: (a) Additive low-rank difference, which LoRA can effectively compensate for the difference. (b) Orthogonal rotation, which follows the assumption of OFT and is full-rank. (c) True fully fine-tuned weights, which could be mixtures of additive and rotative effects.

SDXL [40] model and the fine-tuned SDXL-Inpaint [50] model. We consider three settings: (a) Additive low-rank difference, where the desired weight  $\mathbf{W}_*$  is generated by some low-rank update  $\mathbf{W}_* = \mathbf{W}_0 + \mathbf{B}_* \mathbf{A}_*$ . (b) Orthogonal rotation, where the desired weight  $\mathbf{W}_*$  is generated by an orthogonal transform  $\mathbf{W}_* = \mathbf{W}_0 \mathbf{T}_*$ . (c) True fully fine-tuned weight, where  $\mathbf{W}_*$  is obtained by full-parameter fine-tuning, which is identical to SDXL-Inpaint [50]. We approximate  $\mathbf{W}_*$  using: (I) OFT in Eq. (2). (II) LoRA in Eq. (1). (III) TR, which replaces  $\Delta$  in Eq. (1) with TR. (IV) OFT + LoRA, which uses OFT for  $\mathbf{T}$  and LoRA for  $\Delta$  in Eq. (3). (V) TRM + LoRA, which uses TRM for  $\mathbf{T}$  and LoRA for  $\Delta$  in Eq. (3). (VI) TRM + TR, which uses TRM for  $\mathbf{T}$  and TR for  $\Delta$  in Eq. (3). To showcase the expressiveness, we illustrate the approximation error with different adaptation budgets in Fig. 2. More details and results on different layers/models can be found in Appendix A. Based on the results, we have several observations.

- LoRA and OFT work well under their own assumptions, i.e. Figs. 2a and 2b respectively, which may not hold in the real case (Fig. 2c). Adding the TRM transform can take the best of both worlds and performs well across these settings. More importantly, the TRM transform generally improves LoRA and TR in Figs. 2b and 2c.
- Compared to LoRA, the TR can be advantageous when the parameter budget is extremely small. In Fig. 2c, TRM + TR achieves comparable error with LoRA  $R = 1$  (the leftmost point) using less than 10% sizes. TR can also adapt the budget size more smoothly. However, when the rank increases, the improvement may not be significant.
- The simple combination OFT+LoRA does not reduce the approximation error. In Fig. 2c, it introduces additional parameters compared to LoRA, while the error does not change. We hypothesis this is because that the orthogonal transform does not change the column space spanned by the pre-trained weight, therefore limits the ability to align with the target weight  $\mathbf{W}_*$ .

Although this is a simple simulation study, these observations align well with our experiments in Sec. 4.

### 3.3. Tensor-train matrix transform adaptation

In this subsection, we introduce the structure of the transform  $\mathbf{T}$ . Recall that the purpose of  $\mathbf{T}$  is to align the pre-trained weight  $\mathbf{W}_0$  to the target weight  $\mathbf{W}_*$  as closely as possible, in order to reduce the rank of the residual adaptation  $\Delta$ . Since the target weight space (e.g., optimal weights for the fine-tuning task) is not likely to be low-rank, we assume  $\mathbf{T}$  also has a full-rank structure. Furthermore, to address the sparsity problem in OFT,  $\mathbf{T}$  is expected to have dense entries. As this transform matrix is large, it should be represented by parameter-efficient structures.

To meet the above requirements, we adopt the tensorizing matrix (TRM) form [7, 37, 66]. Given a matrix  $\mathbf{T} \in \mathbb{R}^{I \times J}$ , suppose  $I = \prod_{d=1}^D I_d$ ,  $J = \prod_{d=1}^D J_d$  and that it can be re-arranged (tensorized) into many sub-arrays. The TRM factorizes the matrix into contractions of  $D$  4th-order factors  $\mathbf{A}^d \in \mathbb{R}^{I_d \times J_d \times R_d \times R_{d+1}}$ ,  $\forall d = 1, \dots, D$ , which are called core tensors. The sequence  $[R_1, \dots, R_{D+1}]$  with  $R_{D+1} = R_1$  is the TR rank. When one of the  $R_d$  is equal to 1, TRM reduces to the tensor-train matrix [TTM, 37] form. For simplicity, we assume  $R = R_1 = \dots = R_{D+1}$  and  $I = J$  throughout this work. The TRM assumes each entry of the matrix is computed by,

$$T[i_1 \dots i_D, j_1 \dots j_D] = \text{tr}(\mathbf{A}^1[i_1, j_1, :, :] \dots \mathbf{A}^D[i_D, j_D, :, :]). \quad (4)$$

For simplicity, we denote the TRM format as  $\mathbf{T} = \text{TRM}(\mathbf{A}^{1:D})$ , where  $\mathbf{A}^{1:D}$  denotes  $\{\mathbf{A}^1, \dots, \mathbf{A}^D\}$ .

TRM is a highly compact form for representation of dense and full-rank matrices. If the factors  $\mathbf{A}^{1:D}$  are dense and full-rank, then  $\text{TRM}(\mathbf{A}^{1:D})$  becomes a dense and full-rank matrix. Moreover, the memory cost of the TRM is  $\mathcal{O}(DI^{2/D}R^2)$  if  $I = J$ , which is much lower than the original  $\mathcal{O}(I^2)$  if we adjust proper hyper-parameters  $D$  and  $R$ . To show the expressive power of TRM, we conduct a sim-

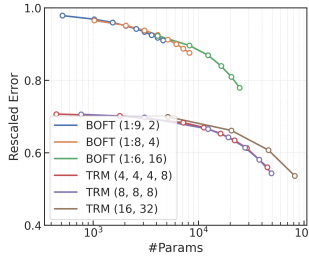


Figure 3. Expressiveness of BOFT and TRM. For BOFT, the first number in the bracket indicates the number of blocks, and the second number indicates the number of Butterfly factors. For TRM, the numbers denote the sizes of sub-indices  $I_d$ .

ulation study to compare it with the Butterfly OFT [BOFT, 28], which is proposed to represent dense matrices in OFT. Specifically, we randomly generate an orthogonal matrix with shape  $512 \times 512$ , and approximate it using BOFT and TRM. The approximation error for different parameter sizes is shown in Fig. 3. TRM achieves a smaller approximation error when the number of parameters is small. Moreover, as we increase the number of parameters, the approximation error of TRM consistently decreases and is better than that of BOFT. More details are provided in Appendix B.

**Initialization.** To ensure that the fine-tuned model is the same as the original model at initialization [18], the transform  $\mathbf{T}$  should be an identity matrix. Fortunately, for TRM, we can easily construct an identity matrix as follows.

**Proposition 1.** *For the TRM in Eq. (4), if we initialize every factor as*

$$\mathbf{A}^d[:, :, r, r'] = \mathbf{I}_{I_d}/R, \forall d = 1, \dots, D, \text{ and } r, r' = 1, \dots, R,$$

*the resulting TRM  $\mathbf{T}$  is an identity matrix.*

**Constrained transform.** While the transform can be powerful, sometimes it is beneficial to have constraints on it, limiting the fine-tuned weight to be within a small region of the pre-trained one. In particular, previous methods adopt identity regularization [41] or orthogonal regularization [3, 29, 61] during fine-tuning. However, directly computing these regularizations on the transform  $\mathbf{T}$  could be computationally expensive. By using the TRM, we show that they can be computed efficiently on the core tensors  $\mathbf{A}^{1:D}$  with much smaller sizes.

For identity regularization  $\|\mathbf{T} - \mathbf{I}_I\|_F$ , we have

$$\mathcal{R}_I(\mathbf{A}^{1:D}) = \sum_{d=1}^D \sum_{r, r'=1}^R \left\| \mathbf{A}^d[:, :, r, r'] - \mathbf{I}_{I_d}/R \right\|_F.$$

According to Prop. 1, this would encourage the transform to be identity. For orthogonal regularization, directly computing  $\|\mathbf{T}\mathbf{T}^\top - \mathbf{I}_I\|_F$  is computationally expensive due to the additional matrix multiplication. Instead, we have

$$\begin{aligned} \mathcal{R}_O(\mathbf{A}^{1:D}) = & \\ & \sum_{d=1}^D \sum_{i_d, j_d=1}^{I_d, I_d} \left\| \sum_{l=1}^{I_d} (\mathbf{A}^d[i_d, l, :, :] \otimes \mathbf{A}^d[j_d, l, :, :]) - \mathbf{I}_{R^2}/R \right\|_F. \end{aligned}$$

**Proposition 2.** *The matrix product of two TRM  $\mathbf{X} = \text{TRM}(\mathbf{A}^{1:D})$  and  $\mathbf{Y} = \text{TRM}(\mathbf{B}^{1:D})$  is still a TRM  $\mathbf{XY}^\top = \text{TRM}(\mathbf{C}^{1:D})$ , where each core tensor satisfies  $\mathbf{C}^d[i_d, j_d, :, :] = \sum_{l_d} \mathbf{A}^d[i_d, l_d, :, :] \otimes \mathbf{B}^d[j_d, l_d, :, :]$  for each  $d = 1, \dots, D$  and  $i_d, j_d = 1, \dots, I_d$ .*

Therefore, combining Props. 1 and 2, we can compute the orthogonal regularization as shown above. In practice, we observe that the identity regularization performs better than the orthogonal regularization. This observation is consistent with the findings in [3, 29, 41].

### 3.4. Tensor-train residual adaptation

Given the powerful transform, we expect the residual part  $\Delta$  in Eq. (3) to be approximated by very compact structures. Specifically, we adopt the tensor-ring (TR) decomposition [66]. Suppose the residual part  $\Delta \in \mathbb{R}^{I \times J}$ , with  $I = \prod_{d=1}^D I_d$ ,  $J = \prod_{d=1}^D J_d$ . The TR format is similar to TRM, but parameterizes the matrix into a more compact and low-rank structure. Specifically, it factorizes the matrix into  $2D$  3rd-order core tensors, denoted as  $\mathbf{B}^d \in \mathbb{R}^{I_d \times R \times R}$  and  $\mathbf{C}^d \in \mathbb{R}^{J_d \times R \times R}, \forall d = 1, \dots, D$ . Each element is computed using the following contraction,

$$\Delta[\overline{i_1 \dots i_D}, \overline{j_1 \dots j_D}] = \text{tr}(\mathbf{B}^1[i_1, :, :] \cdots \mathbf{B}^D[i_D, :, :] \mathbf{C}^1[j_1, :, :] \cdots \mathbf{C}^D[j_D, :, :]). \quad (5)$$

The space complexity is  $\mathcal{O}(DI^{1/D}R^2)$ , which is even smaller than that of TRM.

**Initialization.** Due to the high-order structure, the TR format may be more sensitive to initialization. Previous works adopting TR in PEFT [1, 59] utilize random Gaussian initialization for all factors  $\mathbf{B}^{1:D}$  and  $\mathbf{C}^{1:C}$ , hence losing the zero-initialization of the overall adaptation as in LoRA. This may cause optimization instability and result in the loss of the information from pre-trained models.

In particular, we can write the TR layer as a sequence of linear layers. Given two tensors  $\mathbf{A}$  of shape  $I_d \times R \times R$  and  $\mathbf{X}$  of shape  $I_1 \times \dots \times I_d \times R$ , we define the  $\times_2$  contraction as,

$$\mathbf{A} \times_2 \mathbf{X} = \sum_{l=1}^{I_d} \sum_{r=1}^R \mathbf{A}[l, :, r] \mathbf{X}[I_1, \dots, l, r].$$

The result is of shape  $I_1 \times \dots \times I_{d-1} \times R$ . Therefore, the TR residual layer can be defined as,

$$\text{TR}(\mathbf{B}, \mathbf{C})\mathbf{x} = \text{tr}(\mathbf{B}^1 \cdots \times_2 \mathbf{B}^D \times_2 \mathbf{C}^1 \cdots \times_2 \mathbf{C}^D \times_2 \mathbf{X}),$$

which is reformulated as multiple linear layers. To ensure zero initialization, we initialize  $\mathbf{B}^1$  as a zero tensor. Each element of other core tensors  $\mathbf{B}^{2:D}$  and  $\mathbf{A}^{1:D}$  is initialized independently from Gaussian distribution  $\mathcal{N}(0, \sigma^2)$ . The initialization strategy now basically follows the  $\mu\mathbf{P}$  framework [57], i.e., the standard deviation should be  $\sigma = \Theta(\sqrt{n_{out}}/n_{in})$ , where  $n_{out} = R$  and  $n_{in} = I_d R$ .

### 3.5. Connections with previous methods

In this subsection, we show that some previous methods implicitly or explicitly adopt the idea of a transform to seek a low-rank space. However, instead of using a learnable dense transform such as TRM, they rely on extremely sparse or fixed transforms, which may be insufficient.

**DoRA.** Liu et al. [27] propose to decompose the pre-trained weight  $\mathbf{W}_0$  into magnitude and direction, and fine-tune them separately,

$$\mathbf{W}' = \frac{\mathbf{W}_0 + \mathbf{B}\mathbf{A}}{\|\mathbf{W}_0 + \mathbf{B}\mathbf{A}\|_c} \cdot \text{diag}(\mathbf{m}),$$

where the blue parts  $\mathbf{m} \in \mathbb{R}^{1 \times J}$ ,  $\mathbf{B} \in \mathbb{R}^{I \times R}$  and  $\mathbf{A} \in \mathbb{R}^{R \times J}$  are trainable parameters.  $\|\cdot\|_c$  denotes the column-wise norm. For practical implementation, Liu et al. [27] suggests not updating the norm part and treating it as a constant. Therefore, we omit it and re-write the DoRA as,

$$\mathbf{W}' \propto \mathbf{W}_0 \text{diag}(\mathbf{m}) + \mathbf{B}\mathbf{A} \text{diag}(\mathbf{m}) \approx \mathbf{W}_0 \text{diag}(\mathbf{m}) + \mathbf{B}\mathbf{A}. \quad (6)$$

Here we merge the last  $\mathbf{m}$  into  $\mathbf{A}$  since they are all trainable parameters. Eq. (6) resembles our model Eq. (3) by parameterizing the transform by a diagonal matrix  $\text{diag}(\mathbf{m})$ . Compared to DoRA, TRM is a more flexible dense transform.

**Methods with fixed transform.** Some works assume that the fine-tuning process has better low-rank structures under particular *fixed* transforms. Therefore, they propose to project the adaptation  $\Delta$  using some fixed transforms explicitly or implicitly, such as Fourier low-rank adaptation [4, 11] and low-displacement-rank adaptation [6, 48]. To illustrate this, we take FouRA [4] as an example, which adopts the Discrete Fourier Transform (DFT) on  $\Delta$ , i.e.,  $\Delta_{\text{foura}} = \mathcal{F}^{-1}(\mathbf{B} \cdot \mathcal{F}(\mathbf{A}))$ , where  $\mathcal{F}$  is the DFT. We omit the gating function in FouRA, which could be an orthogonal contribution to the DFT. Empirically, Borse et al. [4, Fig. 4] shows  $\Delta_{\text{foura}}$  has smaller residual singular values than the original LoRA  $\Delta$ , which may explain its better performances. We can consider this as fine-tuning the pre-trained weight under the DFT,

$$\mathbf{y} = \mathcal{F}^{-1}(\mathcal{F}(\mathbf{W}_0) + \mathbf{B} \cdot \mathcal{F}(\mathbf{A}))\mathbf{x},$$

which is essentially learning the low-rank  $\Delta$  in the space of the transformed weight  $\mathcal{F}(\mathbf{W}_0)$ . While this class of methods apply fixed transforms, our method adopts a learnable transform, which would adaptively learn this projection across different models and tasks.

## 4. Experiments

In this section, we present our experimental analysis. More details about settings and results are shown in Appendix C.

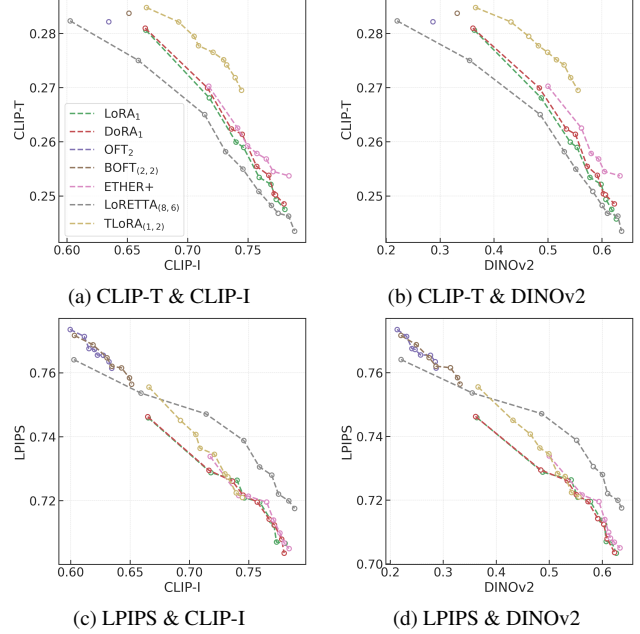


Figure 4. Subject-driven generation results. The larger DINOv2 and CLIP-I values indicate better subject alignment, larger CLIP-T values indicate better prompt alignment and larger LPIPS values indicate larger sample diversity.

### 4.1. Subject-driven generation

**Experimental setting.** We conduct subject-driven generation on the DreamBooth dataset [46]. We fine-tune the SDXL [40] model using the Direct Consistency Optimization [DCO, 23] algorithm. Following previous works [23, 46], we set the batch size to 1 and use the AdamW optimizer with constant learning rates. For all methods, learning rates are tuned from  $\{5e-4, 1e-4, 5e-5\}$ . We train the model for 20 epochs for each individual subject.

**Baselines.** We compare our method with LoRA [18], DoRA [27], OFT [41], BOFT [28], ETHER [3] and LoRETTA [59]. For LoRA and DoRA, the rank is set to 1, to compare performances under extremely limited parameter conditions. The block size is set to be 2 for both OFT and BOFT, while the number of Butterfly factors for BOFT is 2, denoted as OFT<sub>2</sub>, BOFT<sub>(2,2)</sub> respectively. ETHER is a modification of OFT/BOFT by using Householder reflection for orthogonal matrices. For ETHER, we choose the parameterization without orthogonal constraints, denoted as ETHER+, which is reported to have better performance [3]. And the number of blocks is set to 1. For LoRETTA, we choose a LoRA rank of 8 and a TT rank of 6. For our method, we choose TRM transform adaptation with rank 1 and TR residual adaptation with rank 2. The settings and numbers of trainable parameters are shown in Tab. 2. By choosing flexible TRM/TR forms, our method can achieve a much smaller size even compared to LoRA with rank 1.

Table 1. Controllable generation results. We report the mean value of six samples, with the standard deviation in subscripts. Best results are highlighted in bold font. <sup>§</sup>Results are taken from the OFT [41, Table 2] paper. <sup>†</sup>Results are taken from the BOFT [28, Table 6] paper.

Method	#Param (M)	L2I		S2I			C2I	
		Error↓	mIoU↑	aACC↑	mACC↑	IoU↑	F1↑	
SD <sup>§</sup>	0	146.19 <sub>NA</sub>	7.72 <sub>NA</sub>	33.61 <sub>NA</sub>	14.40 <sub>NA</sub>	NA	NA	
ControlNet <sup>§</sup>	361.30	7.61 <sub>NA</sub>	20.88 <sub>NA</sub>	61.42 <sub>NA</sub>	35.52 <sub>NA</sub>	NA	NA	
LoRA <sub>r=4</sub>	0.80	<b>5.32</b> <sub>0.03</sub>	27.72 <sub>0.17</sub>	64.99 <sub>0.26</sub>	40.22 <sub>0.30</sub>	0.180 <sub>3e-4</sub>	0.305 <sub>5e-4</sub>	
LoRETTA <sub>(32, 8)</sub>	0.41	118.14 <sub>0.55</sub>	11.16 <sub>0.36</sub>	40.46 <sub>0.11</sub>	20.27 <sub>0.65</sub>	0.105 <sub>2e-4</sub>	0.189 <sub>3e-4</sub>	
DoRA <sub>r=4</sub>	0.90	6.43 <sub>0.11</sub>	27.11 <sub>0.27</sub>	65.70 <sub>0.37</sub>	39.16 <sub>0.48</sub>	0.143 <sub>4e-4</sub>	0.248 <sub>7e-4</sub>	
ETHER+	0.40	6.40 <sub>0.08</sub>	27.66 <sub>0.29</sub>	65.76 <sub>0.13</sub>	40.37 <sub>0.38</sub>	0.189 <sub>3e-4</sub>	0.317 <sub>4e-4</sub>	
OFT <sub>r=32</sub>	1.50	7.35 <sub>0.07</sub>	28.52 <sub>0.46</sub>	66.04 <sub>0.29</sub>	41.27 <sub>0.54</sub>	0.165 <sub>5e-4</sub>	0.281 <sub>7e-4</sub>	
OFT <sub>r=4</sub> <sup>§</sup>	16.3	7.07 <sub>NA</sub>	27.06 <sub>NA</sub>	62.42 <sub>NA</sub>	40.09 <sub>NA</sub>	NA	NA	
BOFT <sub>(m=2, r=32)</sub>	2.41	7.64 <sub>0.13</sub>	28.45 <sub>0.67</sub>	66.19 <sub>0.47</sub>	41.44 <sub>1.01</sub>	0.161 <sub>4e-4</sub>	0.276 <sub>6e-4</sub>	
BOFT <sub>(m=4, r=8)</sub> <sup>†</sup>	20.76	5.67 <sub>NA</sub>	28.83 <sub>NA</sub>	67.74 <sub>NA</sub>	41.24 <sub>NA</sub>	NA	NA	
TLoRA <sub>(2, 4)</sub> <sup>*</sup>	0.94	<b>5.32</b> <sub>0.10</sub>	<b>29.23</b> <sub>0.43</sub>	<b>69.21</b> <sub>0.17</sub>	<b>41.88</b> <sub>0.84</sub>	<b>0.203</b> <sub>3e-4</sub>	<b>0.337</b> <sub>5e-4</sub>	
TLoRA <sub>(2, 2)</sub> <sup>*</sup>	0.54	5.57 <sub>0.09</sub>	28.29 <sub>0.47</sub>	67.09 <sub>0.37</sub>	40.64 <sub>0.52</sub>	0.160 <sub>2e-4</sub>	0.274 <sub>4e-4</sub>	
TLoRA <sub>(2, 8)</sub>	0.60	5.78 <sub>0.09</sub>	27.42 <sub>0.38</sub>	66.95 <sub>0.21</sub>	38.99 <sub>0.49</sub>	0.178 <sub>3e-4</sub>	0.301 <sub>5e-4</sub>	
TLoRA <sub>(2, 6)</sub>	0.40	5.84 <sub>0.09</sub>	27.03 <sub>0.28</sub>	65.15 <sub>0.31</sub>	38.76 <sub>0.33</sub>	0.184 <sub>4e-4</sub>	0.310 <sub>6e-4</sub>	

Table 2. Number of trainable parameters.

Method	LoRA	DoRA	OFT	BOFT	ETHER+	LoRETTA	TLoRA
Setting	$r=1$	$r=1$	$b=2$	$(m=2, b=2)$	$n=1$	$(8, 6)$	$(1, 2)$
#Param (M)	1.45	2.12	2.24	3.81	1.57	0.99	<b>0.40</b>

**Evaluation.** The performance is evaluated in three aspects: subject alignment, prompt alignment and sample diversity, as in [41]. Specifically, the subject alignment is measured by the image similarity between generated samples and training samples using CLIP-I [42] and DINOv2 [36]. The prompt alignment is measured by the image-text similarity between generated samples and given prompts using CLIP-T [42]. Finally, the sampling diversity is measured by the distances between generated samples and training samples using LPIPS [64]. Note that there are complex trade-offs among these metrics. Typically, during the fine-tuning process, the subject alignment metrics would increase at the cost of losing prompt alignment and sample diversity, due to language shift [46] and over-fitting.

To give a comprehensive visualization of the fine-tuning process, we evaluate the performances every 2 epochs and plot the Pareto curves of these metrics. The numerical evaluation is shown in Fig. 4. Our method achieves the best overall results with the smallest number of parameters. In particular, comparing DoRA with LoRA, we find that adding the magnitude can improve the performance, which is similar to adding the transform part. Moreover, our method further outperforms DoRA, which may be due to the usage of a more effective dense TRM transform. Also, compared to the tensor decomposition baseline LoRETTA, we can see the advantage of using the TRM transform. Interestingly, we find that tensor decomposition methods, in-

cluding LoRETTA and our method, have better sampling diversity in Figs. 4c and 4d.

Qualitative results are illustrated in Fig. 1. We use the same random seeds to generate these images. We find that in many cases, LoRA and DoRA tend to produce similar images. Images from our model sometimes look similar to those from BOFT. However, our model generally has better subject- and text-alignments.

## 4.2. Controllable generation

**Experimental setting.** For controllable generation, we follow the setting in [41, 62]. Specifically, we fine-tune the Stable Diffusion [SD, 44] v1.5 model with datasets of images and conditional signals. Three tasks are evaluated: (1) Landmark to Image (L2I) on the CelebA-HQ [53] dataset, (2) Segmentation to Image (S2I) on the ADE20K [67] dataset, and (3) Canny to Image (C2I) on the ADE20K dataset. The baselines are the same as in Sec. 4.1, with different hyper-parameter settings to adjust the trainable parameters. For our model, we adopt four settings. First, to show the effect of adding the TRM transform adaptation, we apply TRM with rank 2 on top of LoRA with rank 2 and 4, denoted as TLoRA<sub>(2, 2)</sub><sup>\*</sup> and TLoRA<sub>(2, 4)</sub><sup>\*</sup>. Then, we also test TRM with rank 2 and TR residual adaptation with ranks 6 and 8 to achieve a smaller fine-tuning size, denoted as TLoRA<sub>(2, 6)</sub> and TLoRA<sub>(2, 8)</sub> respectively.

**Results.** For the L2I task, we measure the MSE between the detected face landmark and the ground truth. For the S2I task, we adopt the pre-trained SegFormer B4 model [54] provided in HuggingFace for segmentation of generated images. Then, the mean Intersection over Union (mIoU), all ACC (aACC) and mean ACC (mACC) metrics are reported.

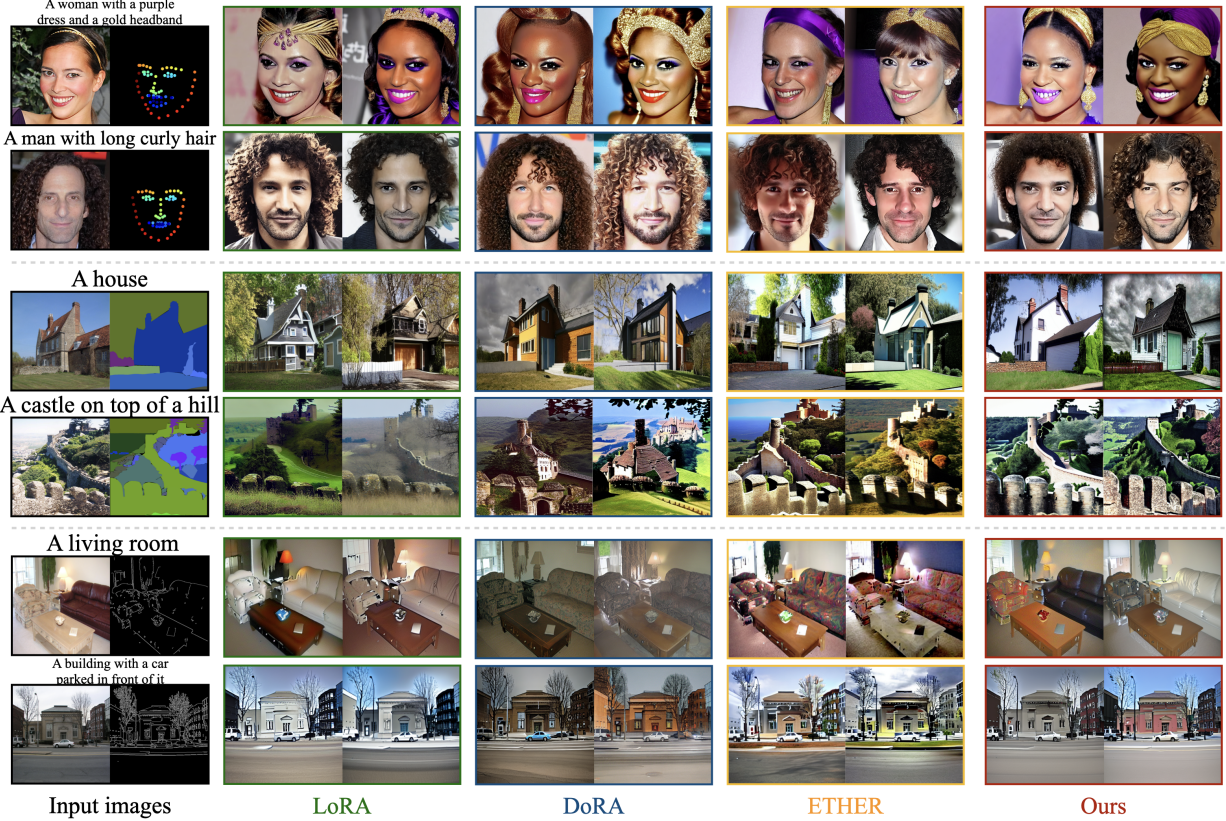


Figure 5. Qualitative results of controllable generation.

For C2I, we evaluate the IoU and F1 score of the Canny edges of generated images. For each test sample, we generate six images to report the mean and standard deviation.

The numerical results are shown in Tab. 1. Unlike previous observations in [28, 41], we find LoRA is actually a strong baseline for these tasks. Nonetheless, our model achieves the best or comparable results. For the L2I task, we find LoRA achieves the best performance. DoRA is inferior to LoRA for this task, which may indicate that the transform part is not important here. However, our model can still achieve a comparable performance. For S2I and C2I tasks, our method by adding the transform significantly improves performances. Unlike in Sec. 4.1, since here we use larger ranks, the TR residual does not have advantages in L2I and S2I tasks, which is consistent with our observations in Sec. 3.2. Moreover, we find LoRETTA is very unstable for these datasets. It either diverges or generates unrealistic images. This may be because of its non-zero initialization, which destroys the information from the pre-trained model. As a comparison, our method, which also adopts TR residual adaptation, works well for these datasets.

Fig. 5 showcases test examples and generated images. Our model also achieves good signal alignment, prompt alignment and image quality. For instance, in the L2I task, our model not only generates images aligned with the face

landmark, but also preserves good prompt alignment. In the S2I task, LoRA generates images with lower signal alignment, which is consistent with the numerical results. In the C2I task, the image quality of LoRA is not good, although it achieves high accuracy on control signals.

## 5. Conclusion and discussion

In this work, we investigate the PEFT problem for text-to-image (T2I) models. Our objective is to address the issues of LoRA regarding its low-rank assumption and inflexible parameter budget choices. Our proposed PEFT method incorporates two adaptation parts, the transform and residual adaptations. We adopt efficient and flexible tensor decomposition (TD) structures for these parts to meet different requirements. Empirically, this combination of transforms and residuals shows advantages in approximation and fine-tuning T2I models for different tasks.

While we focus on T2I models, the proposed method is general for PEFT of other tasks. Moreover, TD is particularly suitable for convolutional layers, whose weights are naturally multi-way arrays. In the future, we plan to test our method on other foundation models, including large-language models and vision transformers.

## References

[1] V Abronin, A Naumov, D Mazur, D Bystrov, K Tsarova, Ar Melnikov, I Oseledets, Sergey Dolgov, R Brasher, and Michael Perelshtain. Tqcompressor: improving tensor decomposition methods in neural networks via permutations. *arXiv preprint arXiv:2401.16367*, 2024. 5

[2] Afia Anjum, Maksim E Eren, Ismael Boureima, Boian Alexandrov, and Manish Bhattacharai. Tensor train low-rank approximation (tt-lora): Democratizing ai with accelerated llms. *arXiv preprint arXiv:2408.01008*, 2024. 2, 3, 9

[3] Massimo Bini, Karsten Roth, Zeynep Akata, and Anna Khoreva. Ether: Efficient finetuning of large-scale models with hyperplane reflections. In *Forty-first International Conference on Machine Learning*. 3, 5, 6, 4, 9

[4] Shubhankar Borse, Shreya Kadambi, Nilesh Prasad Pandey, Kartikeya Bhardwaj, Viswanath Ganapathy, Sweta Priyadarshi, Risheek Garrepalli, Rafael Esteves, Munawar Hayat, and Fatih Porikli. Foura: Fourier low rank adaptation. *arXiv preprint arXiv:2406.08798*, 2024. 2, 3, 6, 9

[5] Adrian Bulat and Georgios Tzimiropoulos. How far are we from solving the 2d & 3d face alignment problem? (and a dataset of 230,000 3d facial landmarks). In *International Conference on Computer Vision*, 2017. 4, 5

[6] Zhuo Chen, Rumen Dangovski, Charlotte Loh, Owen Dugan, Di Luo, and Marin Soljačić. Quanta: Efficient high-rank fine-tuning of llms with quantum-informed tensor adaptation. *arXiv preprint arXiv:2406.00132*, 2024. 2, 3, 6, 9

[7] Andrzej Cichocki, Namgil Lee, Ivan Oseledets, Anh-Huy Phan, Qibin Zhao, and Danilo P Mandic. Tensor networks for dimensionality reduction and large-scale optimization: Part 1 low-rank tensor decompositions. *Foundations and Trends® in Machine Learning*, 9(4-5):249–429, 2016. 2, 3, 4, 9

[8] Patrick Esser, Sumith Kulal, Andreas Blattmann, Rahim Entezari, Jonas Müller, Harry Saini, Yam Levi, Dominik Lorenz, Axel Sauer, Frederic Boesel, et al. Scaling rectified flow transformers for high-resolution image synthesis. In *Forty-first International Conference on Machine Learning*, 2024. 2, 9

[9] Vlad Fomenko, Han Yu, Jongho Lee, Stanley Hsieh, and Weizhu Chen. A note on lora. *arXiv preprint arXiv:2404.05086*, 2024. 2, 3, 9

[10] Rinon Gal, Yuval Alaluf, Yuval Atzmon, Or Patashnik, Amit Haim Bermano, Gal Chechik, and Daniel Cohen-or. An image is worth one word: Personalizing text-to-image generation using textual inversion. In *The Eleventh International Conference on Learning Representations*, 2023. 2, 9

[11] Ziqi Gao, Qichao Wang, Aochuan Chen, Zijing Liu, Bingzhe Wu, Liang Chen, and Jia Li. Parameter-efficient fine-tuning with discrete fourier transform. In *Forty-first International Conference on Machine Learning*, 2024. 2, 3, 6, 9

[12] Timur Garipov, Dmitry Podoprikhin, Alexander Novikov, and Dmitry Vetrov. Ultimate tensorization: compressing convolutional and fc layers alike. *arXiv preprint arXiv:1611.03214*, 2016. 3, 9

[13] Ian Goodfellow. Deep learning book notation. [https://github.com/goodfeli/dlbook\\_notation](https://github.com/goodfeli/dlbook_notation). 3

[14] Ian Goodfellow, Yoshua Bengio, and Aaron Courville. *Deep Learning*. MIT Press, 2016. <http://www.deeplearningbook.org>. 3

[15] Yuchao Gu, Xintao Wang, Jay Zhangjie Wu, Yujun Shi, Yunpeng Chen, Zihan Fan, Wuyou Xiao, Rui Zhao, Shuning Chang, Weijia Wu, et al. Mix-of-show: Decentralized low-rank adaptation for multi-concept customization of diffusion models. *Advances in Neural Information Processing Systems*, 36, 2024. 2, 3, 9

[16] Ligong Han, Yinxiao Li, Han Zhang, Peyman Milanfar, Dimitris Metaxas, and Feng Yang. Svdiff: Compact parameter space for diffusion fine-tuning. In *Proceedings of the IEEE/CVF International Conference on Computer Vision*, pages 7323–7334, 2023. 3, 9

[17] Neil Houlsby, Andrei Giurgiu, Stanislaw Jastrzebski, Bruna Morrone, Quentin De Laroussilhe, Andrea Gesmundo, Mona Attariyan, and Sylvain Gelly. Parameter-efficient transfer learning for nlp. In *International conference on machine learning*, pages 2790–2799. PMLR, 2019. 3, 9

[18] Edward J Hu, yelong shen, Phillip Wallis, Zeyuan Allen-Zhu, Yuanzhi Li, Shean Wang, Lu Wang, and Weizhu Chen. LoRA: Low-rank adaptation of large language models. In *International Conference on Learning Representations*, 2022. 2, 3, 5, 6, 4, 9

[19] Nam Hyeon-Woo, Moon Ye-Bin, and Tae-Hyun Oh. Fedpara: Low-rank hadamard product for communication-efficient federated learning. In *International Conference on Learning Representations*, 2022. 3

[20] Shibo Jie and Zhi-Hong Deng. Fact: Factor-tuning for lightweight adaptation on vision transformer. In *Proceedings of the AAAI conference on artificial intelligence*, pages 1060–1068, 2023. 3, 9

[21] Dawid Jan Kopiczko, Tijmen Blankevoort, and Yuki M Asano. Vera: Vector-based random matrix adaptation. In *The Twelfth International Conference on Learning Representations*. 3, 9

[22] Nupur Kumari, Bingliang Zhang, Richard Zhang, Eli Shechtman, and Jun-Yan Zhu. Multi-concept customization of text-to-image diffusion. In *Proceedings of the IEEE/CVF Conference on Computer Vision and Pattern Recognition*, pages 1931–1941, 2023. 2, 9

[23] Kyungmin Lee, Sangkyung Kwak, Kihyuk Sohn, and Jinwoo Shin. Direct consistency optimization for compositional text-to-image personalization. *arXiv preprint arXiv:2402.12004*, 2024. 6, 4

[24] Brian Lester, Rami Al-Rfou, and Noah Constant. The power of scale for parameter-efficient prompt tuning. In *Proceedings of the 2021 Conference on Empirical Methods in Natural Language Processing*. Association for Computational Linguistics, 2021. 3, 9

[25] Junnan Li, Dongxu Li, Caiming Xiong, and Steven Hoi. Blip: Bootstrapping language-image pre-training for unified vision-language understanding and generation. In *International conference on machine learning*, pages 12888–12900. PMLR, 2022. 4

[26] Xiang Lisa Li and Percy Liang. Prefix-tuning: Optimizing continuous prompts for generation. In *Proceedings of*

*the 59th Annual Meeting of the Association for Computational Linguistics and the 11th International Joint Conference on Natural Language Processing (Volume 1: Long Papers)*, pages 4582–4597, 2021. 3, 9

[27] Shih-yang Liu, Chien-Yi Wang, Hongxu Yin, Pavlo Molchanov, Yu-Chiang Frank Wang, Kwang-Ting Cheng, and Min-Hung Chen. DORA: Weight-decomposed low-rank adaptation. In *Forty-first International Conference on Machine Learning*, 2024. 2, 3, 6, 4, 9

[28] Weiyang Liu, Zeju Qiu, Yao Feng, Yuliang Xiu, Yuxuan Xue, Longhui Yu, Haiwen Feng, Zhen Liu, Juyeon Heo, Songyou Peng, Yandong Wen, Michael J. Black, Adrian Weller, and Bernhard Schölkopf. Parameter-efficient orthogonal finetuning via butterfly factorization. In *The Twelfth International Conference on Learning Representations*, 2024. 2, 3, 5, 6, 7, 8, 4, 9

[29] Xinyu Ma, Xu Chu, Zhibang Yang, Yang Lin, Xin Gao, and Junfeng Zhao. Parameter efficient quasi-orthogonal finetuning via givens rotation. In *Forty-first International Conference on Machine Learning*. 3, 5, 9

[30] Xindian Ma, Peng Zhang, Shuai Zhang, Nan Duan, Yuexian Hou, Ming Zhou, and Dawei Song. A tensorized transformer for language modeling. *Advances in neural information processing systems*, 32, 2019. 3, 9

[31] Sourab Mangrulkar, Sylvain Gugger, Lysandre Debut, Younes Belkada, Sayak Paul, and Benjamin Bossan. Peft: State-of-the-art parameter-efficient fine-tuning methods. <https://github.com/huggingface/peft>, 2022. 4

[32] Ronak Mehta, Rudrasis Chakraborty, Yunyang Xiong, and Vikas Singh. Scaling recurrent models via orthogonal approximations in tensor trains. In *Proceedings of the IEEE/CVF International Conference on Computer Vision*, pages 10571–10579, 2019. 3, 9

[33] Chong Mou, Xintao Wang, Liangbin Xie, Yanze Wu, Jian Zhang, Zhongang Qi, and Ying Shan. T2i-adapter: Learning adapters to dig out more controllable ability for text-to-image diffusion models. In *Proceedings of the AAAI Conference on Artificial Intelligence*, pages 4296–4304, 2024. 2

[34] Mahdi Nikdan, Soroush Tabesh, Elvir Crnčević, and Dan Alistarh. RoSA: Accurate parameter-efficient fine-tuning via robust adaptation. In *Forty-first International Conference on Machine Learning*, 2024. 2, 3, 9

[35] Alexander Novikov, Dmitrii Podoprikhin, Anton Osokin, and Dmitry P. Vetrov. Tensorizing neural networks. *Advances in neural information processing systems*, 28, 2015. 3, 9

[36] Maxime Oquab, Timothée Darcet, Théo Moutakanni, Huy Vo, Marc Szafraniec, Vasil Khalidov, Pierre Fernandez, Daniel Haziza, Francisco Massa, Alaaeldin El-Nouby, et al. Dinov2: Learning robust visual features without supervision. *Transactions on Machine Learning Research Journal*, pages 1–31, 2024. 7

[37] Ivan V Oseledets. Tensor-train decomposition. *SIAM Journal on Scientific Computing*, 33(5):2295–2317, 2011. 2, 3, 4, 9

[38] Yu Pan, Jing Xu, Maolin Wang, Jinmian Ye, Fei Wang, Kun Bai, and Zenglin Xu. Compressing recurrent neural networks with tensor ring for action recognition. In *Proceedings of the AAAI Conference on Artificial Intelligence*, pages 4683–4690, 2019. 3, 9

[39] Hoang Pham Minh, Nguyen Nguyen Xuan, and Son Tran Thai. Tt-vit: Vision transformer compression using tensor-train decomposition. In *International Conference on Computational Collective Intelligence*, pages 755–767. Springer, 2022. 3, 9

[40] Dustin Podell, Zion English, Kyle Lacey, Andreas Blattmann, Tim Dockhorn, Jonas Müller, Joe Penna, and Robin Rombach. SDXL: Improving latent diffusion models for high-resolution image synthesis. In *The Twelfth International Conference on Learning Representations*, 2024. 2, 4, 6, 9

[41] Zeju Qiu, Weiyang Liu, Haiwen Feng, Yuxuan Xue, Yao Feng, Zhen Liu, Dan Zhang, Adrian Weller, and Bernhard Schölkopf. Controlling text-to-image diffusion by orthogonal finetuning. *Advances in Neural Information Processing Systems*, 36:79320–79362, 2023. 3, 5, 6, 7, 8, 1, 4, 9

[42] Alec Radford, Jong Wook Kim, Chris Hallacy, Aditya Ramesh, Gabriel Goh, Sandhini Agarwal, Girish Sastry, Amanda Askell, Pamela Mishkin, Jack Clark, et al. Learning transferable visual models from natural language supervision. In *International conference on machine learning*, pages 8748–8763. PMLR, 2021. 7

[43] Aditya Ramesh, Prafulla Dhariwal, Alex Nichol, Casey Chu, and Mark Chen. Hierarchical text-conditional image generation with clip latents. *arXiv preprint arXiv:2204.06125*, 1(2):3, 2022. 2, 9

[44] Robin Rombach, Andreas Blattmann, Dominik Lorenz, Patrick Esser, and Björn Ommer. High-resolution image synthesis with latent diffusion models. In *Proceedings of the IEEE/CVF conference on computer vision and pattern recognition*, pages 10684–10695, 2022. 2, 7, 9

[45] Litu Rout, Yujia Chen, Nataniel Ruiz, Abhishek Kumar, Constantine Caramanis, Sanjay Shakkottai, and Wen-Sheng Chu. Rb-modulation: Training-free personalization of diffusion models using stochastic optimal control. *arXiv preprint arXiv:2405.17401*, 2024. 3, 9

[46] Nataniel Ruiz, Yuanzhen Li, Varun Jampani, Yael Pritch, Michael Rubinstein, and Kfir Aberman. Dreambooth: Fine tuning text-to-image diffusion models for subject-driven generation. In *Proceedings of the IEEE/CVF conference on computer vision and pattern recognition*, pages 22500–22510, 2023. 2, 6, 7, 4, 9

[47] Chitwan Saharia, William Chan, Saurabh Saxena, Lala Li, Jay Whang, Emily L. Denton, Kamyar Ghasemipour, Raphael Gontijo Lopes, Burcu Karagol Ayan, Tim Salimans, et al. Photorealistic text-to-image diffusion models with deep language understanding. *Advances in neural information processing systems*, 35:36479–36494, 2022. 2, 9

[48] Arijit Sehanobish, Avinava Dubey, Krzysztof Choromanski, Somnath Basu Roy Chowdhury, Deepali Jain, Vikas Sindhwani, and Snigdha Chaturvedi. Structured unrestricted-rank matrices for parameter efficient fine-tuning. *arXiv preprint arXiv:2406.17740*, 2024. 2, 3, 6, 9

[49] Jiahao Su, Wonmin Byeon, Jean Kossaifi, Furong Huang, Jan Kautz, and Anima Anandkumar. Convolutional tensor-

train lstm for spatio-temporal learning. *Advances in Neural Information Processing Systems*, 33:13714–13726, 2020. 3, 9

[50] The Diffusers team. SD-XL inpainting 0.1 model card. <https://huggingface.co/diffusers/stable-diffusion-xl-1.0-inpainting-0.1>. 4, 1

[51] Hugo Touvron, Louis Martin, Kevin Stone, Peter Albert, Amjad Almahairi, Yasmine Babaei, Nikolay Bashlykov, Soumya Batra, Prajjwal Bhargava, Shruti Bhosale, et al. Llama 2: Open foundation and fine-tuned chat models. *arXiv preprint arXiv:2307.09288*, 2023. 1

[52] Wenqi Wang, Yifan Sun, Brian Eriksson, Wenlin Wang, and Vaneet Aggarwal. Wide compression: Tensor ring nets. In *Proceedings of the IEEE Conference on Computer Vision and Pattern Recognition*, pages 9329–9338, 2018. 3, 9

[53] Weihao Xia, Yujiu Yang, Jing-Hao Xue, and Baoyuan Wu. Tedigan: Text-guided diverse face image generation and manipulation. In *Proceedings of the IEEE/CVF conference on computer vision and pattern recognition*, pages 2256–2265, 2021. 7, 4

[54] Enze Xie, Wenhui Wang, Zhiding Yu, Anima Anandkumar, Jose M Alvarez, and Ping Luo. Segformer: Simple and efficient design for semantic segmentation with transformers. *Advances in neural information processing systems*, 34: 12077–12090, 2021. 7, 5

[55] Enze Xie, Lewei Yao, Han Shi, Zhili Liu, Daquan Zhou, Zhaoqiang Liu, Jiawei Li, and Zhenguo Li. Diffit: Unlocking transferability of large diffusion models via simple parameter-efficient fine-tuning. In *Proceedings of the IEEE/CVF International Conference on Computer Vision*, pages 4230–4239, 2023. 3, 9

[56] Zeyue Xue, Guanglu Song, Qiushan Guo, Boxiao Liu, Zhuban Zong, Yu Liu, and Ping Luo. Raphael: Text-to-image generation via large mixture of diffusion paths. *Advances in Neural Information Processing Systems*, 36, 2024. 2

[57] Greg Yang, James B Simon, and Jeremy Bernstein. A spectral condition for feature learning. *arXiv preprint arXiv:2310.17813*, 2023. 5

[58] Yinchong Yang, Denis Krompass, and Volker Tresp. Tensor-train recurrent neural networks for video classification. In *International Conference on Machine Learning*, pages 3891–3900. PMLR, 2017. 3, 9

[59] Yifan Yang, Jiajun Zhou, Ngai Wong, and Zheng Zhang. Loretta: Low-rank economic tensor-train adaptation for ultra-low-parameter fine-tuning of large language models. In *Proceedings of the 2024 Conference of the North American Chapter of the Association for Computational Linguistics: Human Language Technologies (Volume 1: Long Papers)*, pages 3161–3176, 2024. 2, 3, 5, 6, 4, 9

[60] SHIH-YING YEH, Yu-Guan Hsieh, Zhidong Gao, Bernard B W Yang, Giyeong Oh, and Yanmin Gong. Navigating text-to-image customization: From lyCORIS fine-tuning to model evaluation. In *The Twelfth International Conference on Learning Representations*, 2024. 3, 9

[61] Shen Yuan, Haotian Liu, and Hongteng Xu. Bridging the gap between low-rank and orthogonal adaptation via householder reflection adaptation. *arXiv preprint arXiv:2405.17484*, 2024. 3, 5, 9

[62] Lvmin Zhang, Anyi Rao, and Maneesh Agrawala. Adding conditional control to text-to-image diffusion models. In *Proceedings of the IEEE/CVF International Conference on Computer Vision*, pages 3836–3847, 2023. 2, 7, 4, 5, 9

[63] Qingru Zhang, Minshuo Chen, Alexander Bukharin, Pengcheng He, Yu Cheng, Weizhu Chen, and Tuo Zhao. Adaptive budget allocation for parameter-efficient fine-tuning. In *International Conference on Learning Representations*. Openreview, 2023. 3, 9

[64] Richard Zhang, Phillip Isola, Alexei A Efros, Eli Shechtman, and Oliver Wang. The unreasonable effectiveness of deep features as a perceptual metric. In *Proceedings of the IEEE conference on computer vision and pattern recognition*, pages 586–595, 2018. 7

[65] Xinxi Zhang, Song Wen, Ligong Han, Felix Juefei-Xu, Akash Srivastava, Junzhou Huang, Hao Wang, Molei Tao, and Dimitris N Metaxas. Spectrum-aware parameter efficient fine-tuning for diffusion models. *arXiv preprint arXiv:2405.21050*, 2024. 3, 4, 9

[66] Qibin Zhao, Guoxu Zhou, Shengli Xie, Liqing Zhang, and Andrzej Cichocki. Tensor ring decomposition. *arXiv preprint arXiv:1606.05535*, 2016. 2, 3, 4, 5, 9

[67] Bolei Zhou, Hang Zhao, Xavier Puig, Sanja Fidler, Adela Barriuso, and Antonio Torralba. Scene parsing through ade20k dataset. In *Proceedings of the IEEE conference on computer vision and pattern recognition*, pages 633–641, 2017. 7, 4

# Transformed Low-rank Adaptation via Tensor Decomposition and Its Applications to Text-to-image Models

## Supplementary Material

### Contents

<b>A Details and more results in Sec. 3.2</b>	<b>1</b>
<b>B Proposed model</b>	<b>1</b>
B.1. Expressiveness of TRM	1
B.2. Proof of Props. 1 and 2	3
<b>C Experiments</b>	<b>4</b>
C.1. Experimental details	4
C.2. Additional visualization results	5
C.3. Failure of LoRETTA	9
<b>D Related work</b>	<b>9</b>

### A. Details and more results in Sec. 3.2

In this section, we present the detailed settings for experiments of approximating fine-tuned weights in Sec. 3.2. Moreover, we provide results of more layers in the SDXL(-Inpaint) models, and models from other domains, e.g., large language models.

First, we present the experimental settings. For results in Fig. 2, the pre-trained weight  $W_0$  is taken from the pre-trained SDXL model and the key for the layer is `mid_block.attentions.0.transformer_blocks.0.attn1.to_k`. The shape of  $W_0$  is  $1280 \times 1280$ . The detailed settings for three cases in Fig. 2 are as follows.

1. **Additive low-rank difference.** The target weight is computed by  $W_* = W_0 + \sigma B_* A_*$ , where the rank of  $B_* A_*$  is 128. Each element of  $B_*$  and  $A_*$  is drawn i.i.d. from  $\mathcal{N}(0, 1)$ . After  $B_*$  and  $A_*$  are generated, we compute  $\sigma$  to scale this difference part so that  $W_* - W_0$  has the same standard deviation with the case where  $W_*$  is the true fully fine-tuned weight from SDXL-Inpaint.
2. **Orthogonal rotation.** The target weight is computed by  $W_* = W_0 T_*$ , where  $T_*$  is a random orthogonal matrix. To generate this orthogonal matrix, we firstly generate a random matrix  $X = I_{1280} + F$ , where each element of  $F$  is drawn i.i.d. from  $\mathcal{N}(0, 0.05^2)$ . Then,  $T_*$  is computed by the QR decomposition of  $X$ .
3. **True fully fine-tuned weight.** The target weight  $W_*$  is taken from the SDXL-Inpaint model [50] in the same layer with  $W_0$ .

All approximation methods are optimized by minimizing the Mean Squared Error (MSE) with Adam optimizer using learning rate  $1e-3$  for 500 epochs, which is sufficient for them to converge. The settings of these methods are as

follows.

- I. **OFT.** We take the block diagonal structure and Cayley transform as in [41]. We vary the block size to get different parameter sizes.
- II. **LoRA.** We vary the rank to get different parameter sizes.
- III. **TR.** We use the TR form defined in Eq. (5) to replace the low-rank matrix decomposition in Eq. (1). The size of the pre-trained weight is  $1280 \times 1280$ . We reshape it into  $1280 = 8 \times 8 \times 4 \times 5$  and choose different TR ranks to get different parameter sizes.
- IV. **OFT + LoRA.** For OFT, we set the block size to 5, and combine it with LoRA of different ranks.
- V. **TRM + LoRA.** We choose TRM with rank 1, and combine it with LoRA of different ranks.
- VI. **TRM + TR.** We choose TRM with rank 1, and combine it with TR of different ranks.

Then, we provide results of different layers in the SDXL(-Inpaints) models in Fig. 6. To investigate the potential application of our method in large language models, we also conduct similar investigations in Llama2 7B and Llama2-chat 7B models [51], as shown in Fig. 7. The size of SDXL weights is  $1280 \times 1280$ , while the size of the Llama2 7B weights is  $4096 \times 4096$ . For both models, we have similar observations as in Sec. 3.2. Moreover, in the SDXL model, we find the effect of adding the transform is more significant for *key* and *query* weights. It would be interesting to analyze this effect more theoretically in the future. Besides, compared to SDXL, the TR structure appears to be more effective in the Llama2 models. This may be because that the tensor decomposition is more suitable for compression of weight matrices with larger sizes. A future direction would be exploration of our method in fine-tuning large language models.

### B. Proposed model

#### B.1. Expressiveness of TRM

In this subsection, we present details of the simulation study in Fig. 3, Sec. 3.3. To empirically compare TRM with Butterly matrices in BOFT, we randomly generate orthogonal matrices and evaluate the approximation error. In specific, we generate a random matrix  $X$  of shape  $512 \times 512$ , where each element is i.i.d. from unit Normal distribution  $\mathcal{N}(0, 1)$ . Then, the target orthogonal matrix  $T_*$  is obtained from the QR decomposition of  $X$ . We approximate  $T_*$  using BOFT and TRM by minimizing the MSE with Adam optimizer.

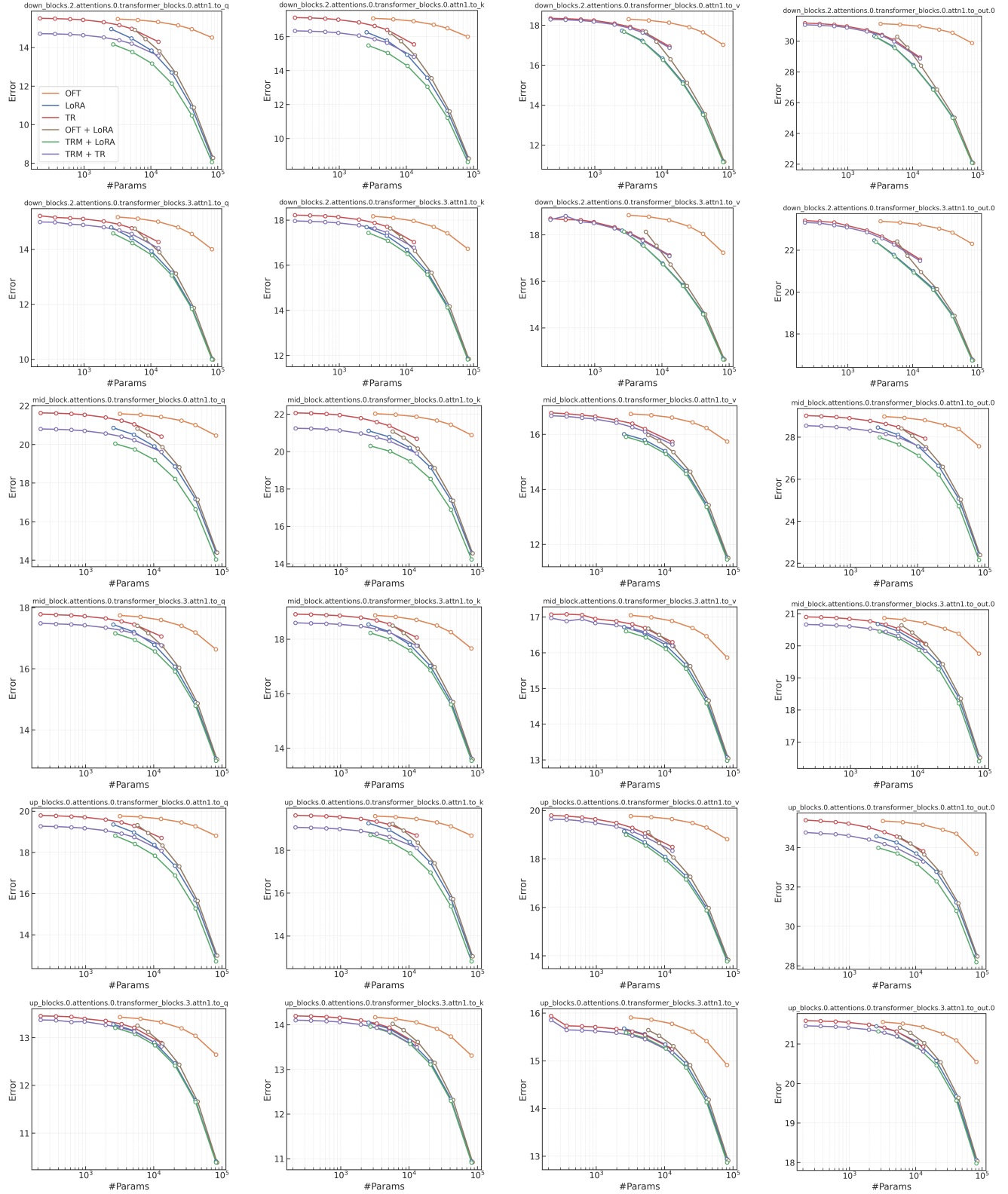


Figure 6. Simulation on different layers of the SDXL and SDXL-Inpaint models.

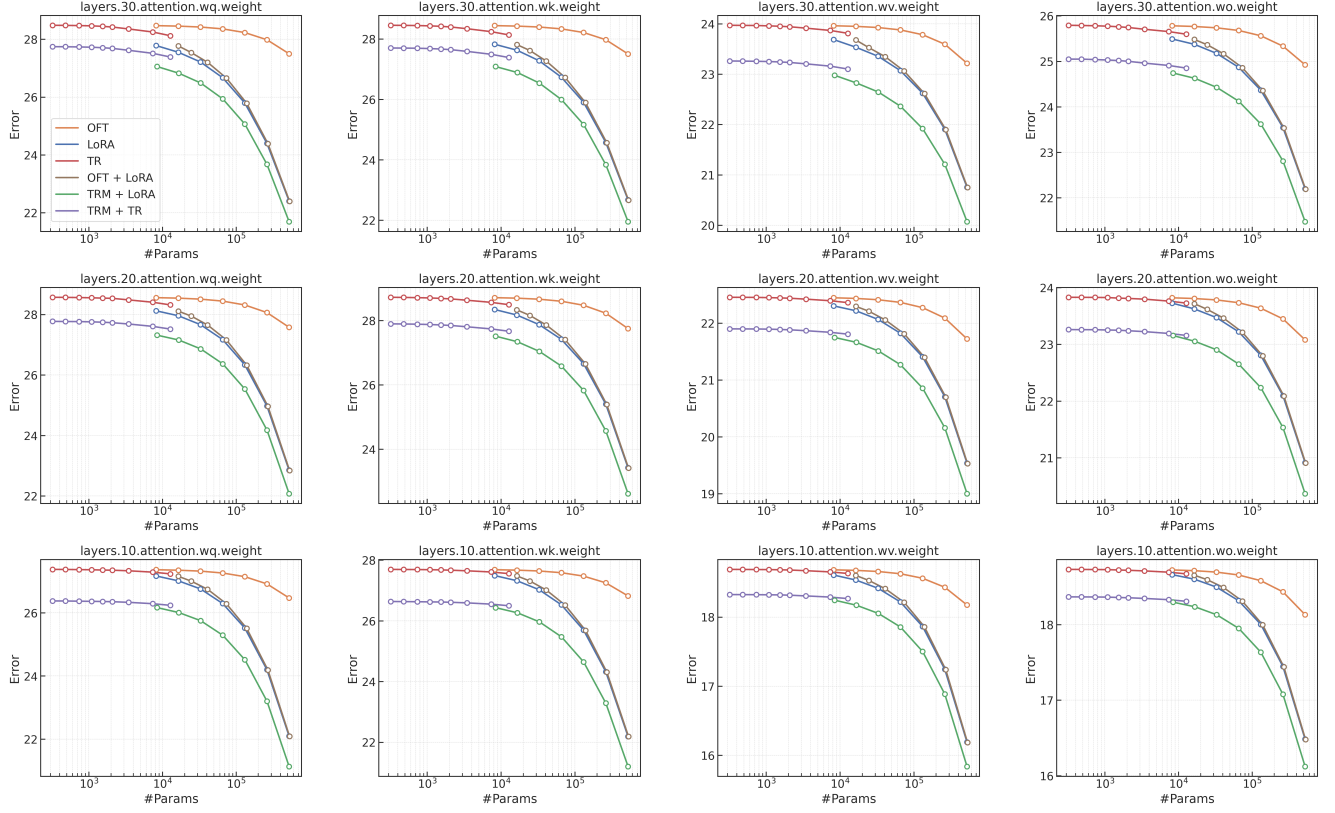


Figure 7. Simulation on different layers of the Llama2 7B and Llama2-chat 7B models.

For BOFT, we test 2, 4, and 16 Butterfly factors, as in [28]. For each setting, we test the number of diagonal blocks ranging from 1 to 9, 1 to 8, and 1 to 6, denoted as BOFT(1:9, 2), BOFT(1:8, 4), and BOFT(1:6, 16) respectively. For TRM, we test different tensor shape, namely,  $4 \times 4 \times 4 \times 8$ ,  $8 \times 8 \times 8$ , and  $16 \times 32$ . Then, we set different TR ranks to obtain results of different parameter sizes. In Fig. 3, we find the results of TRM are robust to the choices of tensor sizes, and are consistently better than BOFT. Besides, even there is no orthogonal constraints for TRM, it can approximate orthogonal matrices well.

## B.2. Proof of Props. 1 and 2

In this subsection, we provide the derivation of Props. 1 and 2.

**Proof of Prop. 1.** According to the definition of TRM in Eq. (4), we have

$$\begin{aligned} \mathbf{T}[\overline{i_1 \cdots i_D}, \overline{j_1 \cdots j_D}] &= \\ \text{tr}(\mathbf{A}^1[i_1, j_1, :, :] \cdots \mathbf{A}^D[i_D, j_D, :, :]). \end{aligned}$$

Following the initialization in Prop. 1, for  $d = 1, \dots, D$ , if  $i_d = j_d$ , all the elements of  $\mathbf{A}^d[i_d, j_d, :, :]$  equal to  $1/R$ ,

else zero. Then we can discuss the diagonal and non-diagonal elements of  $\mathbf{T}$  separately.

1. For non-diagonal elements, i.e.,  $\overline{i_1 \cdots i_D} \neq \overline{j_1 \cdots j_D}$ , there is at least one sub-index  $i_d \neq j_d$ . Therefore,  $\mathbf{T}[\overline{i_1 \cdots i_D}, \overline{j_1 \cdots j_D}] = 0$ , since  $\mathbf{A}^d[i_d, j_d, :, :] = \mathbf{0}$  if  $i_d \neq j_d$ .
2. For diagonal elements, i.e.,  $\overline{i_1 \cdots i_D} = \overline{j_1 \cdots j_D}$ , we have  $i_d = j_d, \forall d = 1, \dots, D$ . Now the core tensors become  $\mathbf{A}^d[i_d, j_d, :, :] = \mathbf{1}_{R \times R}/R, \forall d = 1, \dots, D$  and  $i_d, j_d = 1, \dots, I_d$ , where  $\mathbf{1}_{R \times R}$  is a matrix of shape  $R \times R$  with all elements being one. Therefore,  $\mathbf{T}[\overline{i_1 \cdots i_D}, \overline{j_1 \cdots j_D}] = 1$ , since

$$\text{tr} \left( \frac{\mathbf{1}_{R \times R}}{R} \cdots \frac{\mathbf{1}_{R \times R}}{R} \right) = 1.$$

Therefore,  $\mathbf{T}$  is an identity matrix.

**Proof of Prop. 2.** For simplicity, in this proof, we denote  $\mathbf{A}^d[i_d, j_d] = \mathbf{A}^d[i_d, j_d, :, :]$  and  $\mathbf{B}^d[i_d, j_d] = \mathbf{B}^d[i_d, j_d, :, :]$ . Suppose  $\mathbf{X}$  has shape  $I \times K$  with  $I = \prod_{d=1}^D I_d$  and  $K = \prod_{d=1}^D K_d$ , and  $\mathbf{Y}$  has shape  $J \times K$  with  $J = \prod_{d=1}^D J_d$ . According to the definition of TRM in Eq. (4), we can com-

pute the product  $\mathbf{Z} = \mathbf{X}\mathbf{Y}^\top$  as follows,

$$\begin{aligned}
& \mathbf{Z}[\overline{i_1 \cdots i_D}, \overline{j_1 \cdots j_D}] \\
&= \sum_{k_1, \dots, k_D=1}^{K_1, \dots, K_D} \mathbf{X}[\overline{i_1 \cdots i_D}, \overline{k_1 \cdots k_D}] \mathbf{Y}[\overline{j_1 \cdots j_D}, \overline{k_1 \cdots k_D}] \\
&= \sum_{k_1, \dots, k_D=1}^{K_1, \dots, K_D} \text{tr}(\mathbf{A}^1[i_1, k_1] \cdots \mathbf{A}^D[i_D, k_D]) \\
&\quad \cdot \text{tr}(\mathbf{B}^1[j_1, k_1] \cdots \mathbf{B}^D[j_D, k_D]) \\
&= \sum_{k_1, \dots, k_D=1}^{K_1, \dots, K_D} \text{tr} \left\{ (\mathbf{A}^1[i_1, k_1] \cdots \mathbf{A}^D[i_D, k_D]) \right. \\
&\quad \left. \otimes (\mathbf{B}^1[j_1, k_1] \cdots \mathbf{B}^D[j_D, k_D]) \right\} \\
&= \sum_{k_1, \dots, k_D=1}^{K_1, \dots, K_D} \text{tr} \left\{ (\mathbf{A}^1[i_1, k_1] \otimes \mathbf{B}^1[j_1, k_1]) \right. \\
&\quad \left. \cdots (\mathbf{A}^D[i_D, k_D] \otimes \mathbf{B}^D[j_D, k_D]) \right\} \\
&= \text{tr} \left\{ \sum_{k_1, \dots, k_D=1}^{K_1, \dots, K_D} [(\mathbf{A}^1[i_1, k_1] \otimes \mathbf{B}^1[j_1, k_1]) \right. \\
&\quad \left. \cdots (\mathbf{A}^D[i_D, k_D] \otimes \mathbf{B}^D[j_D, k_D])] \right\} \\
&= \text{tr} \left\{ \sum_{k_1=1}^{K_1} (\mathbf{A}^1[i_1, k_1] \otimes \mathbf{B}^1[j_1, k_1]) \right. \\
&\quad \left. \cdots \sum_{k_D}^{K_D} (\mathbf{A}^D[i_D, k_D] \otimes \mathbf{B}^D[j_D, k_D]) \right\},
\end{aligned}$$

which follows a TR format. Therefore  $\mathbf{X}\mathbf{Y}^\top = \text{TRM}(\mathbf{C}^{1:D})$ , where each core tensor  $\mathbf{C}^d[i_d, j_d, :, :] = \sum_{l_d} (\mathbf{A}^d[i_d, l_d, :, :] \otimes \mathbf{B}^d[j_d, l_d, :, :])$ .

To make  $\mathbf{X}$  orthogonal, i.e.,  $\mathbf{X}\mathbf{X}^\top = \mathbf{I}$ , we can regularize  $\mathbf{C}^{1:D}$  according to the initialization scheme in Prop. 1.

## C. Experiments

In this section, we provide experimental details and more results. All the experiments are conducted on single Nvidia H100 GPUs with 80GB memory.

### C.1. Experimental details

**Datasets.** For the subject-driven generation, we use the DreamBooth dataset [46], which includes 30 subjects from 15 different classes. For text prompts, we follow the setting in Lee et al. [23], Zhang et al. [65]. For each subject, there are several images with 10 testing text prompts. The dataset is available at the Github repository<sup>1</sup> of Zhang et al. [65].

<sup>1</sup><https://github.com/phymhan/SODA-Diffusion>

For the controllable generation task, we consider three tasks and two datasets. The settings basically follow Qiu et al. [41]. For the Landmark to Image (L2I) task, we use the CelebA-HQ [53] dataset. The whole dataset consists of 30k images of faces, captions generated by BLIP [25], and face landmarks detected by the face-alignment library [5]. The test set contains 2987 samples. For the Segmentation to Image (S2I) task, we use the ADE20K 2017 dataset [67], which consists of 20k training images, segmentations and captions generated by BLIP. The test set contains 2000 samples. For the Canny to Image (C2I) task, we also use the ADE20K dataset, where the canny edges are detected using the same detector as in Zhang et al. [62].

**Baselines.** We choose the following baselines, which are highly related to our work and competitive methods.

- LoRA [18], which is the original method.
- DoRA [27], which is a popular extension of LoRA. Moreover, it shares some similarities with our method, as discussed in Sec. 3.5.
- OFT [41], which applies orthogonal transforms for fine-tuning. It uses block diagonal transforms for parameter efficiency.
- BOFT [28], which extends OFT by using Butterfly matrices to construct dense transforms.
- ETHER [3], which adopts Householder reflection to parameterize orthogonal transforms. In particular, we adopt the implementation called ETHER+, which relaxes the orthogonal constraint and applies transforms on the left and right sides of the pre-trained weight. It is more flexible and has shown better results in Bini et al. [3].
- LoRETTA [59], which is an extension of LoRA. It further factorized LoRA matrices using TT decomposition for parameter efficiency.

LoRA, DoRA, OFT, and BOFT are provided in the PEFT library [31]. For ETHER<sup>2</sup> and LoRETTA<sup>3</sup>, we apply their official implementations in our experiments.

**General settings.** For all the baselines and our model, we inject the trainable parameters into the attention modules on *key*, *value*, *query*, and *output* layers. This setting is consistent with previous works [3, 28, 41] for a fair comparison.

For the subject-driven generation, we fine-tune the SDXL [40] model using the Direct Consistency Optimization [DCO, 23] algorithm. Following previous works [23, 46], we set the batch size to 1 and use the AdamW optimizer with constant learning rates. For all methods, learning rates are tuned from  $\{5e-4, 1e-4, 5e-5\}$ . We train the model for 20 epochs for each individual subject.

For the controllable generation, we follow the implementation of ControlNet [62]. It contains a shallow 8-layer

<sup>2</sup><https://github.com/mwbini/ether>

<sup>3</sup><https://github.com/yifanycc/loretta>

Table 3. Hyper-parameters of the subject-driven generation experiment. For OFT,  $b$  means the block size. For BOFT,  $m$  means the number of Butterfly factors and  $b$  means the block size, which is the same with OFT. For ETHER+,  $n$  means the number of blocks. For LoRETTA,  $r_{\text{LoRA}}$  means the rank of LoRA and  $r_{\text{TT}}$  means the rank of TT decomposition. For our method TLoRA,  $r_{\text{TRM}}$  means the rank of the TRM transform and  $r_{\text{TR}}$  means the rank of the TR residual adaptation.

Method	LoRA	DoRA	OFT	BOFT	ETHER+	LoRETTA	TLoRA
Setting	$r=1$	$r=1$	$b=2$	$(m=2, b=2)$	$n=1$	$(r_{\text{LoRA}}=8, r_{\text{TT}}=6)$	$(r_{\text{TRM}}=1, r_{\text{TR}}=2)$
Learning rate	$5e-5$	$5e-5$	$1e-4$	$1e-4$	$5e-4$	$5e-4$	$5e-4$

Table 4. Hyper-parameters of the controllable generation experiment. For OFT,  $b$  means the block size. For BOFT,  $m$  means the number of Butterfly factors and  $b$  means the block size, which is the same with OFT. For ETHER+,  $n$  means the number of blocks. For LoRETTA,  $r_{\text{LoRA}}$  means the rank of LoRA and  $r_{\text{TT}}$  means the rank of TT decomposition. For our method TLoRA,  $r_{\text{TRM}}$  means the rank of the TRM transform,  $r_{\text{LoRA}}$  means the rank of the LoRA residual adaptation and  $r_{\text{TR}}$  means the rank of the TR residual adaptation.  $\lambda$  is the scale of regularization.

Method	LoRA	DoRA	OFT	BOFT	ETHER+	LoRETTA	TLoRA*	TLoRA*	TLoRA	TLoRA
Setting	$r=1$	$r=1$	$b=2$	$(m=2, b=2)$	$n=1$	$(r_{\text{LoRA}}=8, r_{\text{TT}}=6)$	$(r_{\text{TRM}}=2, r_{\text{LoRA}}=2)$	$(r_{\text{TRM}}=2, r_{\text{LoRA}}=4)$	$(r_{\text{TRM}}=2, r_{\text{TR}}=6)$	$(r_{\text{TRM}}=1, r_{\text{TR}}=8)$
Learning rate	$5e-4$	$5e-4$	$1e-4$	$1e-4$	$1e-3$	$1e-5$	$5e-4$	$5e-4$	$1e-3$	$1e-3$
$\lambda$	-	-	-	-	-	-	0	0	$1e-3$	$1e-3$

CNN to encode the control signals. For a fair comparison and being consistent with previous works [3, 28, 41], we report the number of training parameters for adaptation parts of all methods. The optimizer is AdamW. For the CelebA-HQ dataset in the L2I task, the batch size is 16 and we fine-tune the model for 22 epochs. For the ADE20K dataset in the S2I and C2I tasks, the batch size is 8 and we fine-tune the model for 20 epochs. For all methods, learning rates are tuned from  $\{1e-3, 5e-4, 1e-4, 5e-5\}$ . We do some preliminary learning rate search on the L2I and S2I tasks, and find the optimal learning rate of each method is similar for these two tasks. Due to the computational cost, we use the same learning rate for each method on three tasks. Moreover, as the training of LoRETTA is unstable, we additionally adopt a smaller learning rate  $1e-5$  for it.

**Hyper-parameters.** The hyper-parameters for the subject-driven generation is provided in Tab. 3.

The hyper-parameters for the controllable generation is provided in Tab. 4. For this experiment, we find adding the identity regularization  $\mathcal{R}_I$  sometimes helps the performance. We apply a scale  $\lambda$  before adding the regularization on the original loss. The scale  $\lambda$  is chosen from  $\{0, 1e-3\}$ . Moreover, for tensorization of large matrices, we choose the following setting, where the keys are original dimensions and values are dimensions of sub-indices. We do not test other tensorization shapes.

```
TENSOR_SHAPE_DICT = {
    '320': [4, 8, 10], '640': [8, 8, 10],
    '768': [8, 8, 12], '1280': [8, 10, 16],
    '2048': [8, 16, 16], '2560': [10, 16, 16],
    '5120': [20, 16, 16], '10240': [32, 20, 16],
}
```

**Evaluation.** The evaluation of the subject-driven generation is described in Sec. 4.1.

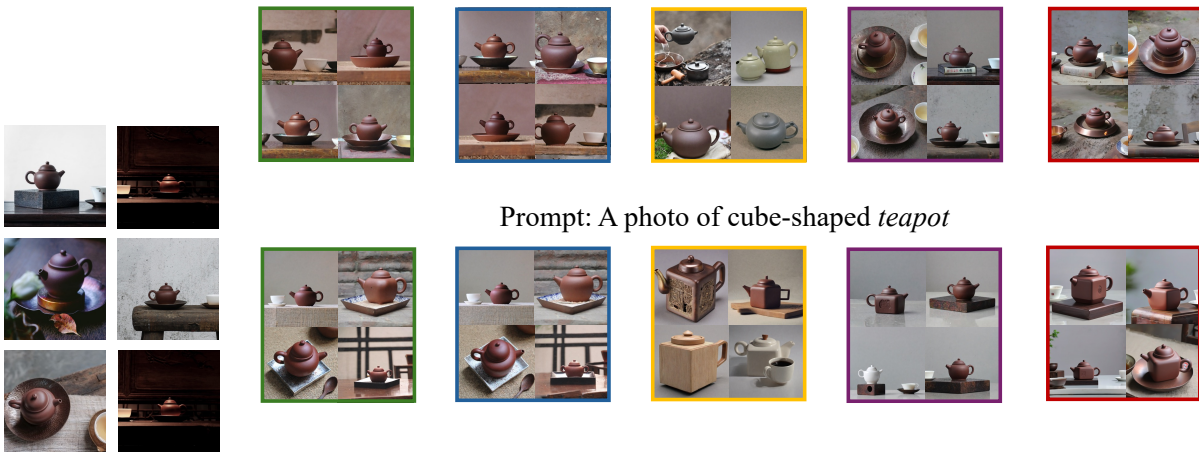
For the L2I task, we use the same face landmark detector provided in the face-alignment library [5] to detect landmarks from generated images. The Mean Squared Error (MSE) between ground truth and detected landmarks is reported. For the S2I task, we adopt the SegFormer B4 model [54] pre-trained on the ADE20K dataset for segmentation of generated images. The model is downloaded from HuggingFace<sup>4</sup>. Then, the mean Intersection over Union (mIoU), all ACC (aACC) and mean ACC (mACC) metrics are reported. For C2I, we compute the canny edges of generate images using the same detector as in [62]. Then, we evaluate the IoU and F1 score of the Canny edges of generated images. For each test sample, we generate six images to report the mean and standard deviation.

## C.2. Additional visualization results

We present more visualization results in Figs. 8 to 10.

<sup>4</sup><https://huggingface.co/nvidia/segformer-b4-finetuned-ade-512-512>

Prompt: A photo of a *teapot*



Prompt: A photo of cube-shaped *teapot*



Prompt: A photo of a transparent *teapot*



Prompt: A *dog2* playing a violin in sticker style



Prompt: A *dog2* carved as a knight in wooden sculpture



Prompt: A photo of a *dog2* as an astronaut in a space suit, walking on the surface of Mars



Input images

LoRA

DoRA

BOFT

ETHER+

Ours

Figure 8. Qualitative comparison of the subject-driven generation results.

Prompt: A vase made of lego



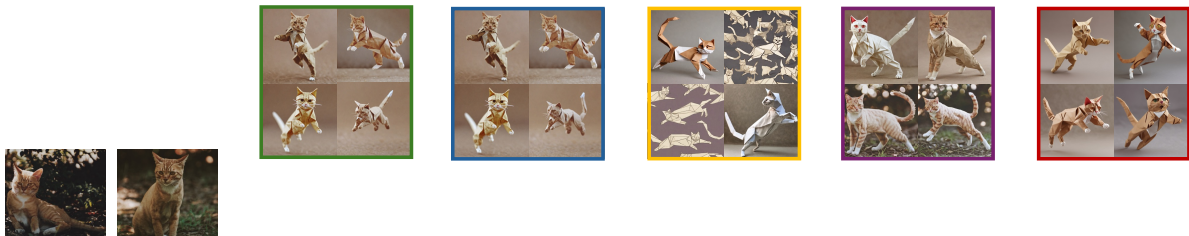
Prompt: A photo of a transparent vase



Prompt: A vase featuring a design inspired by the Arsenal Football Club



Prompt: A cat gracefully leaping in origami style



Prompt: A cat sleeping on a sofa



Prompt: A side view of a cat in times square, looking up at the billboards



Input images

LoRA

DoRA

BOFT

ETHER+

Ours

Figure 9. Qualitative comparison of the subject-driven generation results.

Prompt: A woman wearing glasses



Prompt: A man in a suit and tie



Prompt: A woman with long brown hair



Prompt: A shopping mall



Prompt: A small room with a bed and shelves



Prompt: A person walking down a street



Prompt: A cat in a toilet



Prompt: A bathroom



Prompt: A house in the countryside



Input images

LoRA

DoRA

BOFT

ETHER+

TLoRA\*

TLoRA

Figure 10. Qualitative comparison of the subject-driven generation results.

### C.3. Failure of LoRETTA

When applying the LoRETTA [59] on controllable generation tasks, we find the training is unstable. It either generates unrealistic images or diverges. We test learning rates from  $\{1e-3, 5e-4, 1e-4, 5e-5, 1e-5\}$ . For large learning rates, it diverges quickly, while for small learning rates, it does not learn the control signals well and the image quality is low. To illustrate this, we showcase the training process of LoRETTA on the C2I task in Fig. 11. This may be because of its non-zero initialization, which destroys the information from the pre-trained model. As a comparison, our method, which also adopts TR residual adaptation, works well for these datasets.

## D. Related work

Due to the space limit, we present a more comprehensive review of related work here.

**Text-to-image model personalization.** Text-to-image generative models have shown exceptional results in image synthesis [8, 40, 43, 44, 47]. Given the various pre-trained models available, many works aim to fine-tune these models for personalized datasets or tasks, such as subject-driven generation and controllable generation. Gal et al. [10] propose learning given subjects via textual inversion, while Ruiz et al. [46] fine-tune the whole model. ControlNet [62] incorporates an additional network branch, which can learn datasets of paired control signals and images. While Ruiz et al. [46], Zhang et al. [62] have large numbers of trainable parameters, Kumari et al. [22] show that fine-tuning the attention layers alone is also effective for these tasks. More recently, many works have focused on developing PEFT methods for these attention layers and have shown promising results [4, 15, 16, 41, 55, 60, 65]. There are also training-free approaches [45], which could be slow at inference.

**Parameter-efficient fine-tuning.** PEFT has become a hot topic with the emergence of large foundation models including text-to-image models and large language models. Popular PEFT methods include Adapter [17], Prefix-tuning [26], Prompt-tuning [24], low-rank adaptation [LoRA, 18], and many of their variants. Adapter adds additional layers after pretrained feed forward layers. Prompt-tuning introduces learnable prompts for specific tasks. LoRA has become the most popular PEFT method due to its simplicity and impressive performance [9]. Many variants of LoRA have been proposed [21, 27, 28, 34, 41, 63]. In particular, DoRA [27] proposes decomposing the pre-trained weight into magnitude and direction, where vanilla LoRA is applied to the direction. In this work, we show that DoRA can also be connected to our work by using a diagonal transform. OFT [41] applies a learnable orthogonal transform for

adaptation. However, for parameter efficiency, OFT adopts block diagonal matrices, which are highly sparse. Subsequently, many methods aim to improve OFT by applying more efficient dense transform structures, including Butterfly matrix [28], Given rotation [29], Householder reflection [3, 61] and Kronecker product [65]. Our method adopts a similar idea of using a transform, but we design a different efficient dense matrix parameterization using tensor decomposition. Some methods also share similarities with ours by using *pre-defined and fixed* transforms on the pre-trained weights to project onto some low-rank spaces [4, 11, 48].

**Tensor decomposition.** TD is a classical tool in signal processing and machine learning [7]. In particular, tensor-train (TT) decomposition [37] and its extension, tensor-ring (TR) decomposition [66], have shown exceptional results in model compression, including MLP [35], CNN [12, 52], RNN/LSTM [32, 38, 49, 58] and Transformer [30, 39]. Recently, TDs have also been applied to fine-tuning tasks. Jie and Deng [20] parameterize the Adapter layers using a TT format and show ultra-parameter-efficiency in ViT adaptation. Yang et al. [59] extend this idea to large language model PEFT, and apply the TT format to both Adapters and LoRA factors. Similarly, Anjum et al. [2] propose to directly parameterize the adaptation using the TT format. Chen et al. [6] adopt a quantum-inspired tensor network, which is a generalization of the TT-Matrix (TTM) form. While these works use similar TT/TR structures to our model, they do not apply the transform adaptation. Moreover, we study a different initialization strategy for the TR factors, which would be more stable, as we show in our experiments.

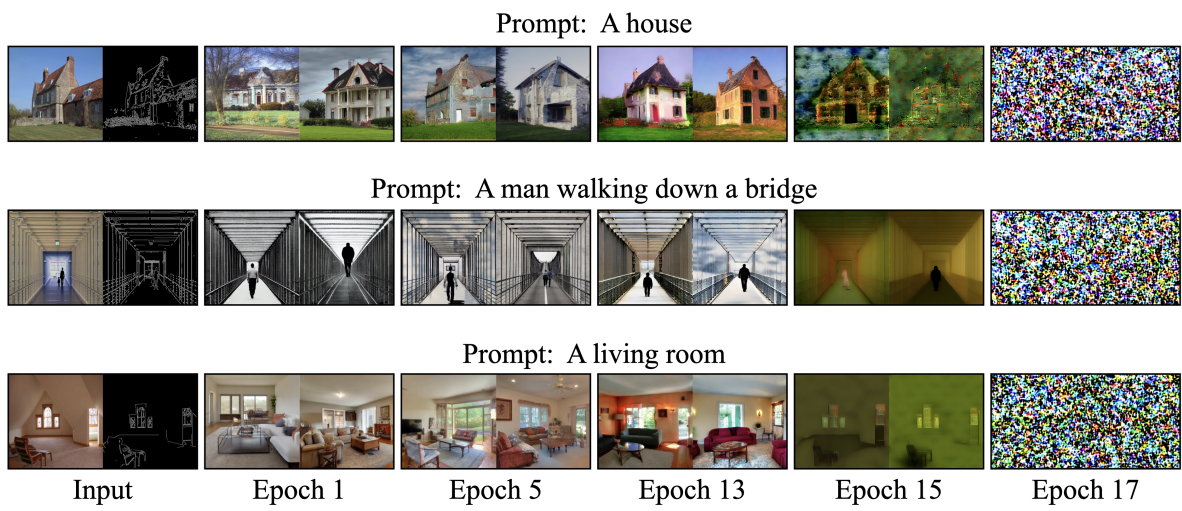


Figure 11. Training process of LoRETTA on the C2I task.